

Mamba-FSCIL: Dynamic Adaptation with Selective State Space Model for Few-Shot Class-Incremental Learning

Xiaojie Li, Yibo Yang, Jianlong Wu, Bernard Ghanem, Liqiang Nie, Min Zhang

Abstract—Few-shot class-incremental learning (FSCIL) confronts the challenge of integrating new classes into a model with minimal training samples while preserving the knowledge of previously learned classes. Traditional methods widely adopt static adaptation relying on a fixed parameter space to learn from data that arrive sequentially, prone to overfitting to the current session. Existing dynamic strategies require the expansion of the parameter space continually, leading to increased complexity. In this study, we explore the potential of Selective State Space Models (SSMs) for FSCIL, leveraging its dynamic weights and strong ability in sequence modeling to address these challenges. Concretely, we propose a dual selective SSM projector that dynamically adjusts the projection parameters based on the intermediate features for dynamic adaptation. The dual design enables the model to maintain the robust features of base classes, while adaptively learning distinctive feature shifts for novel classes. Additionally, we develop a class-sensitive selective scan mechanism to guide dynamic adaptation. It minimizes the disruption to base-class representations caused by training on novel data, and meanwhile, forces the selective scan to perform in distinct patterns between base and novel classes. Experiments on miniImageNet, CUB-200, and CIFAR-100 demonstrate that our framework outperforms the existing state-of-the-art methods. The code is available at <https://github.com/xiaojieli0903/Mamba-FSCIL>.

Index Terms—Few-Shot Class Incremental Learning, Selective State Space Model, Dynamic Adaptation, Class Incremental Learning



1 INTRODUCTION

DEEP neural networks often struggle with adapting to new scenarios from limited data without forgetting previous knowledge. This is particularly challenging in real-time environments like robotics and autonomous driving, where data arrives incrementally and new categories often have few samples to learn. To address this challenge, the concept of few-shot class-incremental learning (FSCIL) was introduced [1], [2], [3]. In FSCIL, a model is trained on a base session with sufficient labels and samples. Subsequently, it must adapt to new classes encountered in later sessions, each containing only a few examples, without access to the data from previous sessions. Critically, the model needs to accurately classify images from all encountered classes in each session’s evaluation, balancing the adaptation to new classes with retaining knowledge of previously learned classes.

Various methods have been developed to address FSCIL [4], [5]. Data-based methods [6], [7], [8] replay data subsets or create synthetic samples to reinforce memory and mitigate catastrophic forgetting. Optimization-based techniques [9], [10], [11], [12], [13], [14], [15], [16], [17], [18] utilize advanced loss functions, regularization, and pseudo-feature generation to separate old-class and new-

class features. However, most of these methods rely on **static adaptation**, which uses a pre-defined network architecture that does not change dynamically in response to new information. For example, as shown in Figure 1 (a), multi-layer perceptrons (MLPs) are usually used to project features from the frozen backbone to prototype classifiers [8], [16], [19]. While computationally efficient, MLP cannot dynamically adjust its parameters as class distributions evolve over different learning sessions. As a result, it has insufficient capacity to manage the delicate balance between preserving old knowledge (stability) and accommodating new ability (plasticity), leading to inferior performance on new classes or catastrophic forgetting of old ones. Dynamic network-based methods [1], [2], [20], [21], [22], [23], [24], [25], [26] offer an alternative by expanding architectures with each incremental session. They introduce extra task-specific parameters while preserving the parameters related to the old classes. While enhancing the capacity to incorporate new knowledge, these methods often require continuous structural changes and parameter expansion, leading to increased complexity and resource demands in incremental training.

Recently, Selective State Space Models (SSMs) [27], as known as the Mamba model, have emerged as a compelling alternative to self-attention mechanisms [28], [29], [30] to efficiently handle long sequences. Mamba introduces a selective scan mechanism that dynamically computes its system matrices based on the input context, allowing for the effective handling of diverse and evolving data characteristics. This **dynamic adaptation** enables Mamba to adjust its operation parameters according to the needs of different input distributions, increasing the compatibility between

- X. Li, J. Wu, L. Nie, and M. Zhang are with the School of Computer Science and Technology, Harbin Institute of Technology (Shenzhen), 518055, China. E-mail: xiaojieli0903@gmail.com, wujianlong@hit.edu.cn, nieliqiang@gmail.com, zhangmin2021@hit.edu.cn.
- Y. Yang and B. Ghanem are with King Abdullah University of Science and Technology, Jeddah, Saudi Arabia. Email: yibo.yang93@gmail.com, bernard.ghanem@kaust.edu.sa

FSCIL by proposing a dual selective SSM projector. The dual design maintains the base-class features and adaptively adjusts its projection parameters based on the input context for dynamic adaptation on novel classes, mitigating catastrophic forgetting and enhancing adaptability.

- We further develop a class-sensitive selective scan mechanism to guide the dynamic adaptation composed of two loss terms. The suppression loss minimizes the disruption to old-class representations caused by incremental training, maintaining stability for base classes. The separation loss makes the selective scan perform in distinct patterns to induce plasticity for novel classes.
- Our approach is thoroughly evaluated on standard FSCIL benchmarks, including CIFAR-100, CUB-200, and miniImageNet. Our results achieve state-of-the-art performances, demonstrating effectiveness in improving and preserving base-class accuracy and enhancing the adaptability to novel classes.

2 RELATED WORK

2.1 Few-Shot Learning (FSL)

FSL enables models to classify new classes with limited training samples [40], [41], [42], [43], and can be divided into four main strategies: data augmentation, metric-based, model-based, and optimization-based approaches [44]. *Data augmentation methods* reduce overfitting and enhance generalization by increasing data diversity through transforming existing samples or synthetic data generation using models like VAEs or GANs [45]. *Metric-based methods* classify objects by computing similarity or distance between samples in a learned embedding space, with common approaches including Siamese Networks [46], Matching Networks [47], and Prototypical Networks [48]. *Model-based methods* design specific architectures for FSL challenges, such as Memory-Augmented Neural Networks [49] and Meta Networks [50], to store crucial class information and learn generalizable meta-knowledge. *Optimization-based methods* aim for fast model adaptation with few-shot data. Model-Agnostic Meta-Learning (MAML) [51] is a common optimization algorithm that trains the model’s initial parameters using various datasets to ensure a peak performance when tackling new tasks. Reptile [52] extends MAML by simplifying gradient calculations, enhancing computational efficiency.

While FSL focuses on generalizing to new classes with limited data, it does not prioritize retaining knowledge of base classes. In contrast, FSCIL requires models to continuously learn new classes with limited samples while preserving the knowledge of previously learned classes.

2.2 Class-Incremental Learning (CIL)

CIL enables models to learn new classes over time without forgetting previously acquired knowledge [53], [54], [55], [56], [57], [9], [24], [58]. CIL approaches include non-exemplar-based and exemplar-based methods. *Non-exemplar-based methods* focus on preserving existing knowledge without relying on stored examples. Methods like EWC [59], MAS [60], and SI [61] measure the importance of parameters and apply regularization to prevent significant

changes in critical parameters. Additionally, some methods dynamically change the model architecture, using network expansion and pruning to accommodate new tasks [62], [63], [22]. *Exemplar-based methods*, e.g., iCaRL [55], combine exemplar replay with knowledge distillation, while BiC [64] forms a validation set from saved exemplars and adjusts outputs via a scaling layer. GEM [65], [66] uses exemplars for gradient projection to prevent knowledge overwriting. Additional approaches include storing embeddings rather than raw images [67], using generative models for replay [68], and implementing task-wise adaptation and output normalization [69], [70], [71], [72].

While CIL typically has sufficient training data in incremental sessions, FSCIL complicates this by limiting training samples, making the prevention of catastrophic forgetting even more difficult.

2.3 Few-shot Class-Incremental Learning (FSCIL)

FSCIL [4], [5] combines the aspects of FSL and CIL, continuously learning new classes with a small number of samples to a model’s knowledge base over time without retraining from scratch. FSCIL faces the key challenges: (1) *Catastrophic Forgetting*. Learning new classes without accessing the data of old classes can cause the model to forget previously acquired knowledge [73], [74], [75]. (2) *Data Scarcity*. Limited data availability hampers the model’s ability to learn robust and generalizable representations and increases the overfitting risk [48], [76]. (3) *Stability-Plasticity Dilemma*. The model must seek a delicate balance, maintaining the knowledge of old classes while adapting to the new ones [77], [78], [79].

Various methods have been proposed to address the challenges. *Data-based strategies* mitigate catastrophic forgetting by replaying a subset of real data or generating synthetic data [6], [7], [8]. *Optimization-based methods* adopt techniques like meta-learning [20], [17], [18], pseudo-feature generation [80], [3], advanced loss functions or regularizers [9], [14], [15], [11], [12], [81], [82], [83], [84], well-designed classifiers [16], [19], [85], [86], [87], and knowledge distillation [1], [13], [10], [88]. For example, C-FSCIL [16] employs a mapping strategy that transforms input images into quasi-orthogonal prototypes to enhance class separability. NC-FSCIL [19] introduces a fixed equiangular tight frame classifier and trains a projection layer to attract the backbone features to these ideal prototypes, thus mitigating inter-class interference. However, most of these methods are based on static adaptation, whose parameters are not aware of the input, increasing the difficulty of striving for a comprehensive ability in both old and new classes. *Dynamic adaptation methods* dynamically adjust the model structure or interrelationships between prototypes [1], [21], [22], [23], [2], [89]. TOPIC [1] uses a neural gas network to integrate new nodes and edges for new classes. CEC [2] employs graph models to evolve the classifier’s topology as new classes emerge. Dynamic networks such as LEC-Net [21], DER [22], DSN [23] and FeSSS [89] introduce task-specific parameters for new tasks while preserving those related to old tasks.

Different from these approaches that often require expanding the parameter space, our method achieves dynamic adaptation leveraging the Selective SSM mechanism in Mamba that adjusts parameters based on input characteristics without increasing model complexity.

2.4 State Space Models

Transformers [28], [29], [30], despite their proficiency in handling long-range dependencies, are hindered by their quadratic computational cost with respect to input size and large inference-time memory requirements from the key-value cache, particularly for long sequences or high-resolution images. In contrast, State Space Models (SSMs) provide an efficient alternative, capable of processing extensive sequences with significantly reduced computational demands [90], [91], [92], [93], [94], [95], [96], [97], [98], [99]. SSMs involve recurrent updates over a sequence through hidden states, maintaining context in hidden states, and updating outputs by integrating these states with incoming inputs. Structured state space models (S4) [90], [91] exemplify this efficiency with a parameterized linear recurrent neural network. Subsequent research further enhances computational efficiency and expressive capacity of SSMs across various applications [91], [92], [93], [94], [95].

Mamba [27], [100] enhances S4 with a data-dependent selective mechanism to selectively propagate or forget information according to sequential input tokens and proposes hardware-aware algorithms to boost efficiency. Mamba has also been adopted to process non-sequential input such as images and videos in vision tasks [31], [35], [33], [34], [37], [38], [36], [39]. Among them, VMamba [31] introduces a cross-scan mechanism that processes images in both horizontal and vertical dimensions, allowing feature map elements to integrate information from all directions and providing a global receptive field without increasing linear computational complexity.

Although the Mamba model has been extensively applied in various domains such as text [27], [96], [90], [101], vision [35], [31], [36], [102], audio [103], its potential to mitigate model forgetting has not yet been explored. This study is the first attempt to apply Mamba in FSCIL, effectively harnessing its capabilities of dynamic adaptation and sequence modeling to achieve state-of-the-art performance.

3 PRELIMINARIES

3.1 Few-Shot Class-Incremental Learning

FSCIL trains a model incrementally in multiple sessions $\{\mathcal{D}^{(0)}, \mathcal{D}^{(1)}, \dots, \mathcal{D}^{(T)}\}$, where $\mathcal{D}^{(t)} = \{(x_i, y_i)\}_{i=1}^{|\mathcal{D}^{(t)}|}$ represents the training set for session t . $\mathcal{D}^{(0)}$ is the base session, and T is the number of incremental sessions. The base session $\mathcal{D}^{(0)}$ usually contains a large label space $\mathcal{C}^{(0)}$ and extensive training data for each class $c \in \mathcal{C}^{(0)}$. In each incremental session $\mathcal{D}^{(t)}$, $t > 0$, there are only a few labeled images, $|\mathcal{D}^{(t)}| = pq$, where p is the number of classes and q is the number of samples per novel class, known as p -way q -shot. There is no overlap in the label space between sessions *i.e.*, $\mathcal{C}^{(t)} \cap \mathcal{C}^{(t')} = \emptyset$ for all $t' \neq t$. The training sets from previous sessions are not accessible, which requires the model to generalize to new data without forgetting previously learned information. Evaluation in session t involves test data from all classes encountered up to that session, *i.e.*, the label space of $\cup_{i=0}^t \mathcal{C}^{(i)}$.

3.2 Mamba

State Space Models (SSMs) map the input sequence $x(t) \in \mathbb{R}^L$ to the output sequences $y(t) \in \mathbb{R}^L$ through a recurrently updated hidden state $h(t) \in \mathbb{R}^D$, formulated as:

$$h'(t) = \mathbf{A}h(t) + \mathbf{B}x(t), \quad y(t) = \mathbf{C}h(t), \quad (1)$$

where $\mathbf{A} \in \mathbb{R}^{D \times D}$ is the system's evolution matrix, and $\mathbf{B} \in \mathbb{R}^{D \times 1}$, $\mathbf{C} \in \mathbb{R}^{1 \times D}$ are the projection matrix. To adapt this continuous system for practical implementation, the structured state space model (S4) [90] and Mamba [27] employ the discretization transformation by zero-order hold rule, using a timescale parameter $\Delta \in \mathbb{R} > 0$ to transform the continuous parameters to discrete counterparts:

$$\begin{aligned} \bar{\mathbf{A}} &= \exp(\Delta \mathbf{A}), \\ \bar{\mathbf{B}} &= (\Delta \mathbf{A})^{-1}(\exp(\Delta \mathbf{A}) - \mathbf{I}) \cdot \Delta \mathbf{B}. \end{aligned} \quad (2)$$

The discretized system is defined as:

$$h_t = \bar{\mathbf{A}}h_{t-1} + \bar{\mathbf{B}}x_t, \quad y_t = \mathbf{C}h_t. \quad (3)$$

This system enables efficient global convolution operations that can be processed in parallel:

$$\bar{\mathbf{K}} = (\mathbf{C}\bar{\mathbf{B}}, \mathbf{C}\bar{\mathbf{A}}\bar{\mathbf{B}}, \dots, \mathbf{C}\bar{\mathbf{A}}^{L-1}\bar{\mathbf{B}}), \quad \mathbf{y} = \mathbf{X} * \bar{\mathbf{K}}, \quad (4)$$

where $*$ denotes convolution operation, and $\bar{\mathbf{K}} \in \mathbb{R}^L$ is a convolutional kernel that covers the entire input sequence with the length of L . However, the current system employs constant operation parameters, *e.g.*, \mathbf{C} and \mathbf{B} , which remain static for varying input. This mechanism prevents S4 from selecting the correct information from the context or affecting the hidden state in an input-dependent manner.

Selective State Space Models (S6) are the core component of Mamba, enhancing S4 by introducing a selective and dynamic mechanism for the interactions between sequential states [27]. Unlike conventional SSMs that utilize constant operation matrices that are agnostic of input features, S6 models utilize input-dependent parameters that calculate parameters \mathbf{B} , \mathbf{C} , and Δ directly from the input sequence \mathbf{x} through linear projections, enabling a dynamic and context-aware adaptation to the unique characteristics of the data.

2D Selective Scan (SS2D) enhances Mamba's ability to effectively capture spatial information for vision tasks [31]. SS2D arranges the feature patches in four different directions (top-left to bottom-right, bottom-right to top-left, top-right to bottom-left, and bottom-left to top-right), creating four separate sequences. Each sequence is processed by the S6 module before merging to reconstruct the 2D feature map. Given the input feature \mathbf{z} , the output feature $\bar{\mathbf{z}}$ of SS2D is formulated as:

$$\bar{\mathbf{z}} = \text{SS2D}(\mathbf{z}) = \sum_{i=1}^K \text{S6}(\text{scan}(\mathbf{z}, i)), \quad (5)$$

where $\text{scan}(\mathbf{z}, i)$ converts feature patches into a sequence according to direction i , and K denotes the number of scan paths (default is 4). This approach ensures the comprehensive integration of contextual information from all directions, enhancing the model's global receptive field.

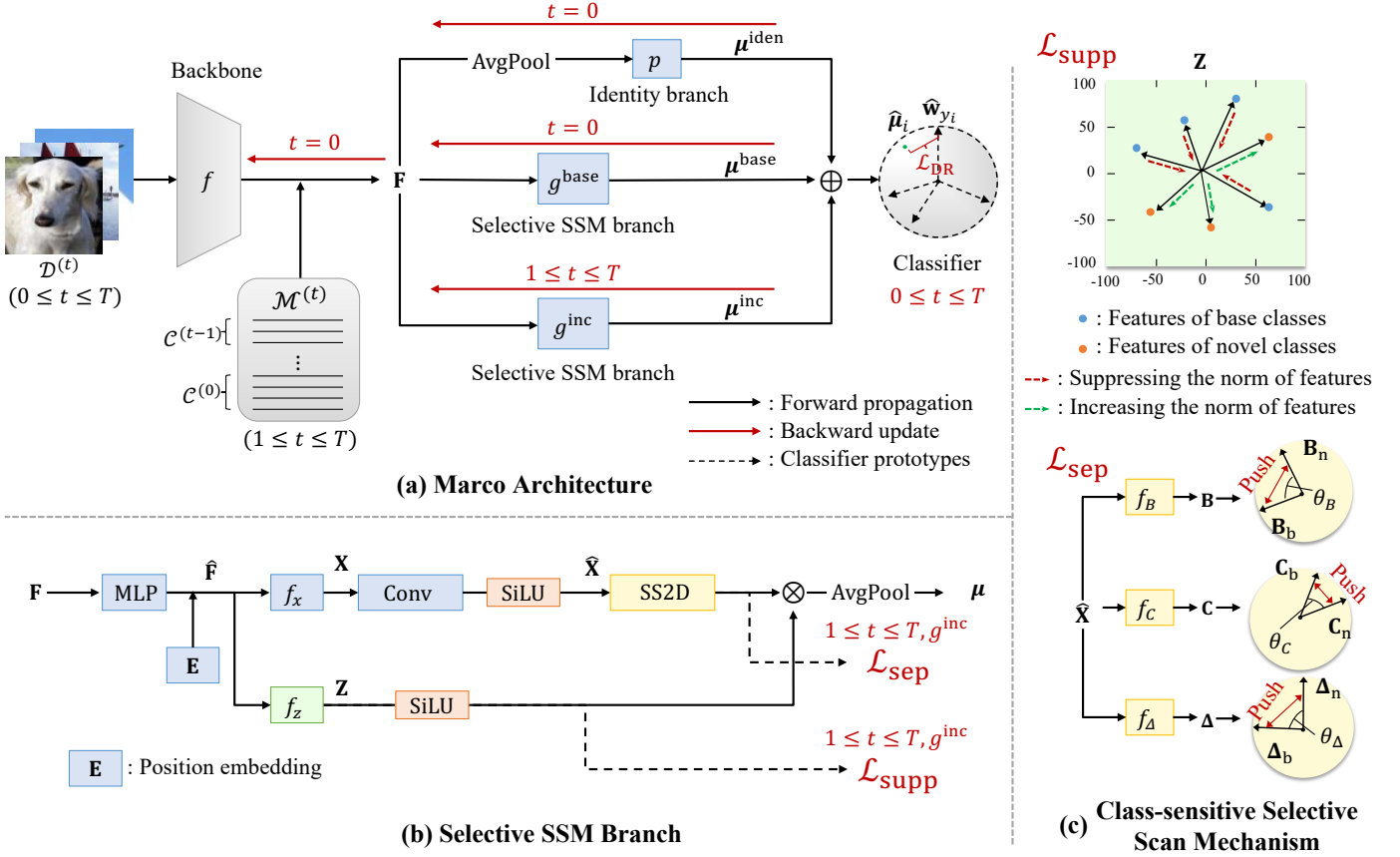


Fig. 2: Mamba-FSCIL framework. The macro architecture (a) is composed of a backbone network f , a dual selective SSM projector consisting of an identity branch p and two selective SSM branches (g^{base} for the base session and g^{inc} for incremental sessions) with the identical structure of (b), and a classifier. Our class-sensitive selective scan (c) performs $\mathcal{L}_{\text{supp}}$ and \mathcal{L}_{sep} in the incremental selective SSM branch g^{inc} to guide the dynamic adaptation in incremental session's training.

4 MAMBA-FSCIL

4.1 Macro Architecture

The architecture of Mamba-FSCIL, illustrated in Fig. 2 (a), is composed of a backbone network f , a dual selective SSM projector, and a linear classifier. The backbone network f processes the input x to generate intermediate features $\mathbf{F} = f(x) \in \mathbb{R}^{N \times D \times H \times W}$, where N , D , H , and W denote the batch size, number of channels, height, and width, respectively. It is only trainable in the base session to learn a powerful feature extractor from the extensive base session data and is then frozen during incremental sessions, a common practice in FSCIL [2], [19], [104], [83] to prevent catastrophic forgetting caused by fine-tuning on novel classes.

We develop a dual selective SSM projector that maps the frozen intermediate features into the final representation for dynamic adaptation. It consists of three branches: a base session branch g^{base} , an incremental session branch g^{inc} , and an identity branch p . The base session branch and incremental session branch have the same structure shown in Fig. 2 (b). The base session branch is responsible for projecting the features of the base classes into a stable and robust representation, which is frozen during the incremental sessions. The incremental session branch dynamically adapts to new classes by learning feature shifts while preserving the

previously learned knowledge. The details of this projector will be introduced in Section 4.2.

To further enhance dynamic adaptation, a class-sensitive selective scan mechanism is proposed. This mechanism guides the incremental session branch g^{inc} in adapting to new classes with minimal interference to the representations of base classes. As shown in Fig. 2 (c), it employs suppression and separation losses to manage the impact of new classes and enforce distinct patterns of feature adaptation between base and novel classes. This mechanism will be detailed in Section 4.3.

The classifier adopts a fixed simplex equiangular tight frame (ETF) following [19], [105], [106], [107], [108], [109]. It provides an ideal feature space arrangement with the maximal equiangular separation among classes [110], [111]. In Section 4.4, we will introduce the training and optimization process across sessions.

4.2 Dual Selective SSM Projector

As illustrated in Figure 2, a backbone network produces the intermediate feature \mathbf{F} . The dual selective SSM projector is composed of three branches: an identity branch, and two selective SSM branches. The identity branch processes \mathbf{F} through $\mu^{\text{iden}} = p(\text{AvgPool}(\mathbf{F}))$, where AvgPool is the average pooling function, p is linear projection operation. In the selective SSM branch for the base session (g^{base}), as

shown in Fig. 2 (b), \mathbf{F} is first reshaped from a 2D feature map into a sequence of flattened feature vectors to be processed by an MLP layer and is added with the position embedding as:

$$\hat{\mathbf{F}}^{\text{base}} = \text{MLP}(\text{Reshape}(\mathbf{F})) + \mathbf{E}^{\text{base}}, \quad (6)$$

where $\mathbf{E}^{\text{base}} \in \mathbb{R}^{L \times D'}$ denotes the position embedding, $\hat{\mathbf{F}}^{\text{base}} \in \mathbb{R}^{N \times L \times D'}$ is the output feature, D' denotes the output dimension, and $L = H \times W$ denotes the total number of spatial locations. Then $\hat{\mathbf{F}}^{\text{base}}$ goes through a selective SSM module, which splits the features into two information streams via linear projections f_x and f_z , creating $\mathbf{X}^{\text{base}} = f_x(\hat{\mathbf{F}}^{\text{base}})$ and $\mathbf{Z}^{\text{base}} = f_z(\hat{\mathbf{F}}^{\text{base}})$. \mathbf{X}^{base} is intended for scanning, while \mathbf{Z}^{base} is used for gating the output of the scanned results. Specifically, the \mathbf{X}^{base} stream is then enhanced through a group convolution function followed by a SiLU activation function:

$$\hat{\mathbf{X}}^{\text{base}} = \text{SiLU}(\text{Conv}(\mathbf{X}^{\text{base}})). \quad (7)$$

The enhanced features $\hat{\mathbf{X}}^{\text{base}}$ are then processed by the SS2D module defined in Eq. (5), enhancing discrimination and stability crucial for maintaining high accuracy within base classes. The output of the selective SSM branch μ^{base} is obtained by elementwise multiplication of the output of the SS2D module and \mathbf{Z}^{base} (after applying the SiLU activation) with average pooling:

$$\mu^{\text{base}} = \text{AvgPool}(\text{SS2D}(\hat{\mathbf{X}}^{\text{base}}) \otimes \text{SiLU}(\mathbf{Z}^{\text{base}})), \quad (8)$$

where \otimes denotes elementwise multiplication. The SS2D system matrices for the input features $\hat{\mathbf{X}}^{\text{base}}$ are calculated by linear projections as:

$$\mathbf{B} = f_B(\hat{\mathbf{X}}^{\text{base}}), \quad \mathbf{C} = f_C(\hat{\mathbf{X}}^{\text{base}}), \quad \mathbf{\Delta} = f_{\Delta}(\hat{\mathbf{X}}^{\text{base}}), \quad (9)$$

where $\mathbf{B} \in \mathbb{R}^{N \times K \times D_B \times L}$, $\mathbf{C} \in \mathbb{R}^{N \times K \times D_C \times L}$, $\mathbf{\Delta} \in \mathbb{R}^{N \times K \times D_{\Delta} \times L}$ are data-dependent system matrices, with K representing the number of scan directions in Eq. (5). Here, D_* represents the dimensions of each parameter. Then, the final representation of the base session is obtained by combining the outputs of the identity branch and the selective SSM branch as:

$$\mu^{(0)} = \mu^{\text{base}} + \mu^{\text{idn}}. \quad (10)$$

During the base session, the backbone network and the selective SSM branch g^{base} use the abundant available data to learn robust feature representations, thus laying a powerful feature extractor for later incremental training. Due to the huge gap in training data between the base session and incremental sessions, a single selective SSM is difficult to achieve a universal dynamic adaptation for all the base and incremental classes. To this end, our dual selective SSM projector adopts another selective SSM branch (g^{inc}) with an identical structure for incremental sessions.

Concretely, in each incremental session $1 \leq t \leq T$, the backbone network f , the identity branch p , and the selective SSM branch for the base session g^{base} are frozen, and only the newly introduced g^{inc} is learnable to adapt the model to novel classes. Following the widely adopted practice in FSCIL [10], [11], [12], [16], [19], [82], we employ a memory module $\mathcal{M}^{(t)}$, which stores the mean intermediate

feature \mathbf{F}_c of each old class c to alleviate forgetting when encountering novel classes:

$$\begin{aligned} \mathcal{M}^{(t)} &= \{\mathbf{F}_c \mid c \in \cup_{j=0}^{t-1} \mathcal{C}^{(j)}\}, \\ \mathbf{F}_c &= \text{Avg}_i \{f(\mathbf{x}_i) \mid y_i = c\}. \end{aligned} \quad (11)$$

The intermediate features of the new class data, along with the stored mean features of the old classes, are processed through p and g^{base} to produce μ^{idn} and μ^{base} respectively, using the same processes as in the base session. Additionally, these features are processed through g^{inc} to generate the output:

$$\mu^{\text{inc}} = \text{AvgPool}(\text{SS2D}(\hat{\mathbf{X}}^{\text{inc}}) \otimes \text{SiLU}(\mathbf{Z}^{\text{inc}})), \quad (12)$$

where $\hat{\mathbf{X}}^{\text{inc}}$ and \mathbf{Z}^{inc} are processed using the same architecture as the base branch g^{base} , but with different parameters. The resulting final representation for incremental sessions is aggregated as:

$$\mu^{(t)} = \mu^{\text{base}} + \mu^{\text{inc}} + \mu^{\text{idn}}, \quad t \geq 1. \quad (13)$$

In this way, the branch g^{inc} learns the shifts of feature distribution prompted by the new class data upon the robust representation established during the base session to dynamically accommodate the model to new classes. It enhances the adaptation ability of the model without altering the previously learned knowledge badly under the guidance of our class-sensitive selective scan.

4.3 Class-sensitive Selective Scan

In this section, we develop a class-sensitive selective scan mechanism, as illustrated in Fig. 2 (c) that guides the dynamic adaptation of the incremental selective SSM branch g^{inc} by two loss terms: suppression loss ($\mathcal{L}_{\text{supp}}$) and separation loss (\mathcal{L}_{sep}).

Suppression Loss ($\mathcal{L}_{\text{supp}}$). This loss focuses on adjusting the norm of the feature vector \mathbf{Z}^{inc} , depicted in the top part of Fig. 2 (c). The diagram shows the distribution of features for the base (blue dots) and novel (orange dots) classes, with dashed lines representing the intention of modifying feature norms. In Eq. (12), the feature vector \mathbf{Z}^{inc} plays a pivotal role in the elementwise multiplication with outputs from the SS2D module. By adjusting the norm of \mathbf{Z}^{inc} , we intend to manipulate the magnitude of the resulting feature vector μ^{inc} , which serves as a class-sensitive gating mechanism that controls the impact of new features with respect to base classes and incremental classes differently during incremental session training:

- **For base classes**, the norm of \mathbf{Z}^{inc} of base classes is suppressed (red dashed lines) to decrease μ^{inc} 's magnitude, thus minimizing feature shifts caused by the new branch g^{inc} to maintain the stability of the features of the base classes.
- **For novel classes**, conversely, the norm of \mathbf{Z}^{inc} is increased (green dashed lines) to enhance μ^{inc} 's magnitude, facilitating the learning of feature shifts that help the model adapt to new classes.

Therefore, the suppression loss can be formulated as:

$$\begin{aligned}\mathcal{L}_{\text{supp}}^{\text{base}} &= \sum_{(\mathbf{F}_c, y_c) \in \mathcal{M}^{(0)}} \|\mathbf{Z}_c^{\text{inc}}\|^2, \\ \mathcal{L}_{\text{supp}}^{\text{novel}} &= - \sum_{(\mathbf{x}_i, y_i) \in \mathcal{D}^{(t)}} \|\mathbf{Z}_i^{\text{inc}}\|^2 - \sum_{(\mathbf{F}_c, y_c) \in \mathcal{M}^{(t)} \setminus \mathcal{M}^{(0)}} \|\mathbf{Z}_c^{\text{inc}}\|^2,\end{aligned}\quad (14)$$

where $\mathcal{M}^{(t)} \setminus \mathcal{M}^{(0)} = \{\mathbf{F}_c \mid c \in \cup_{j=1}^{t-1} \mathcal{C}^{(j)}\}$, and we have:

$$\mathcal{L}_{\text{supp}} = \mathcal{L}_{\text{supp}}^{\text{base}} + \mathcal{L}_{\text{supp}}^{\text{novel}}. \quad (15)$$

By differentially managing the feature magnitudes for base and novel classes through suppression loss, the interference with base-class features brought by the newly added branch g_{inc} is diminished, ensuring that new class integration does not destabilize the model’s existing knowledge. In the ideal case, it is expected that the output of g^{inc} , *i.e.*, $\boldsymbol{\mu}^{\text{inc}}$, could be zero such that the inference of base-class data after incremental session’s training (Eq. (13)) will be equivalent to the one after the base session’s training (Eq. (10)) to induce stability.

Separation Loss (\mathcal{L}_{sep}). The separation term is designed to enhance class sensitivity in the input-dependent parameters (\mathbf{B} , \mathbf{C} , $\boldsymbol{\Delta}$) within the SS2D module, ensuring that base and novel classes are effectively distinguished. As illustrated in the lower part of Fig. 2 (c), the separation mechanism “pushes” the averaged input-dependent parameters associated with novel classes ($\mathbf{B}_n, \mathbf{C}_n, \boldsymbol{\Delta}_n$) away from those of the base classes ($\mathbf{B}_b, \mathbf{C}_b, \boldsymbol{\Delta}_b$), thereby maximizing the distinctiveness between these classes.

Specifically, for both base and novel classes, we calculate their average input-dependent parameters:

$$\begin{aligned}\bar{\mathbf{P}}_b &= \frac{1}{N_{\text{base}} \cdot K \cdot L} \sum_{(\mathbf{F}_i, y_i) \in \mathcal{M}^{(0)}} \sum_{j=1}^K \sum_{k=1}^L \mathbf{P}_{i,j,;,k}, \\ \bar{\mathbf{P}}_n &= \frac{1}{N_{\text{novel}} \cdot K \cdot L} \sum_{\mathcal{D}^{(t)} \cup (\mathcal{M}^{(t)} \setminus \mathcal{M}^{(0)})} \sum_{j=1}^K \sum_{k=1}^L \mathbf{P}_{i,j,;,k},\end{aligned}\quad (16)$$

where $\bar{\mathbf{P}}_b$ and $\bar{\mathbf{P}}_n$ represent the aggregated parameters for the base and novel classes, respectively. The symbol \mathbf{P} represents one of \mathbf{B} , \mathbf{C} , or $\boldsymbol{\Delta}$. The terms N_{base} and N_{novel} denote the number of samples in base and novel classes in a mini-batch. To maximize separability, we then compute and minimize the cosine similarity of these averaged parameters between base and novel classes ($\bar{\mathbf{P}}_b$ and $\bar{\mathbf{P}}_n$), which can be formulated as:

$$\mathcal{L}_{\text{sep}} = \frac{\bar{\mathbf{B}}_b \cdot \bar{\mathbf{B}}_n}{\|\bar{\mathbf{B}}_b\| \|\bar{\mathbf{B}}_n\|} + \frac{\bar{\mathbf{C}}_b \cdot \bar{\mathbf{C}}_n}{\|\bar{\mathbf{C}}_b\| \|\bar{\mathbf{C}}_n\|} + \frac{\bar{\boldsymbol{\Delta}}_b \cdot \bar{\boldsymbol{\Delta}}_n}{\|\bar{\boldsymbol{\Delta}}_b\| \|\bar{\boldsymbol{\Delta}}_n\|}. \quad (17)$$

By minimizing \mathcal{L}_{sep} , the selective scan can be performed in distinct patterns between base and novel classes to induce plasticity during incremental learning.

4.4 Optimization

After we get the final representation, *i.e.*, Eq. (10) for the base session and Eq. (13) for incremental sessions, we calculate the classification loss with the ETF classifier. Following [19], [107], we use the *dot regression* (DR) loss [110] as the training objective, as it is shown to outperform cross entropy loss when using a fixed ETF classifier in imbalanced training,

which FSCIL naturally satisfies. The DR loss can be written as:

$$\mathcal{L}_{\text{DR}}(\hat{\boldsymbol{\mu}}_i, \hat{\mathbf{W}}_{\text{ETF}}) = \frac{1}{2} (\hat{\mathbf{w}}_{y_i}^T \hat{\boldsymbol{\mu}}_i - 1)^2, \quad (18)$$

where $\hat{\boldsymbol{\mu}}_i = \frac{\boldsymbol{\mu}_i}{\|\boldsymbol{\mu}_i\|}$ is the l_2 normalized feature of the final representation, y_i is the label of input x_i , and $\hat{\mathbf{w}}_{y_i}$ is the classifier prototype in $\hat{\mathbf{W}}_{\text{ETF}}$ for label y_i .

Base Session Training. During base session training ($t = 0$), the backbone network f , the identity branch p , and the selective SSM branch for the base session g^{base} are jointly optimized to establish a robust feature extractor. The objective during this phase is to minimize the classification loss on the extensive base session dataset:

$$\min_{f, p, g^{\text{base}}} \frac{1}{|\mathcal{D}^{(0)}|} \sum_{(\mathbf{x}_i, y_i) \in \mathcal{D}^{(0)}} \mathcal{L}_{\text{DR}}(\hat{\boldsymbol{\mu}}_i^{(0)}, \hat{\mathbf{W}}_{\text{ETF}}). \quad (19)$$

Incremental Sessions Training. In subsequent sessions ($1 \leq t \leq T$), as new classes are introduced, the optimization of the model focuses on seamlessly integrating these classes while minimizing disruption of previously learned knowledge. The training objective during these sessions is to adapt the model with new-class data and maintain the existing ability of old classes with the stored intermediate features in $\mathcal{M}^{(t)}$. Thus, the classification loss can be formulated as:

$$\mathcal{L}_{\text{cls}}^{(t)} = \frac{1}{|\mathcal{D}^{(t)}| + |\mathcal{M}^{(t)}|} (\mathcal{L}_{\text{cls-new}}^{(t)} + \mathcal{L}_{\text{cls-old}}^{(t)}), \quad (20)$$

where

$$\begin{aligned}\mathcal{L}_{\text{cls-new}}^{(t)} &= \sum_{(\mathbf{x}_i, y_i) \in \mathcal{D}^{(t)}} \mathcal{L}_{\text{DR}}(\hat{\boldsymbol{\mu}}_i^{(t)}, \hat{\mathbf{W}}_{\text{ETF}}), \\ \mathcal{L}_{\text{cls-old}}^{(t)} &= \sum_{(\mathbf{F}_c, y_c) \in \mathcal{M}^{(t)}} \mathcal{L}_{\text{DR}}(\hat{\boldsymbol{\mu}}_c^{(t)}, \hat{\mathbf{W}}_{\text{ETF}}).\end{aligned}\quad (21)$$

Together with the suppression loss and the separation loss in Section 4.3, the total objective in session $t \geq 1$ is:

$$\min_{g^{\text{inc}}} (\mathcal{L}_{\text{cls}}^{(t)} + \alpha \mathcal{L}_{\text{supp}}^{(t)} + \beta \mathcal{L}_{\text{sep}}^{(t)}), \quad (22)$$

where α and β are hyper-parameters to balance the loss scales.

5 EXPERIMENTS

Our experiments evaluate Mamba-FSCIL on the three widely used benchmarks, including miniImageNet [112], CIFAR-100 [113], and CUB-200 [114], comparing it with static and dynamic methods. We conducted ablation studies to analyze the contributions of key components, including the dual selective SSM projector and the class-sensitive selective scan mechanism, as well as the effects of suppression and separation losses on feature alignment and class separability. We also examined the impact of freezing versus training the identity and selective SSM branches, the sensitivity to hyper-parameters, and the influence of varying training samples (shots) and scan paths (K). Additionally, we compared different projection architectures and evaluated Mamba-FSCIL against Dynamic Support Networks (DSN) [23] to demonstrate its efficiency in managing model complexity while achieving superior performance. Finally, we visualized activation maps to further validate the effectiveness of our approach and provided an analysis of feature embeddings.

TABLE 1: FSCIL performance across sessions on miniImageNet compared with other methods. "Average Acc." is the average accuracy across all sessions. "Final Improv." denotes the accuracy improvement of our method in the last session compared to previous methods.

Methods	Venue	Accuracy in each session (%) \uparrow										Average Acc.	Final Improv.
		0	1	2	3	4	5	6	7	8			
<i>Static adaptation methods</i>													
IDLVQ [11]	ICLR 2021	64.77	59.87	55.93	52.62	49.88	47.55	44.83	43.14	41.84	51.16	+17.52	
Self-promoted [86]	CVPR 2021	61.45	63.80	59.53	55.53	52.50	49.60	46.69	43.79	41.92	52.76	+17.44	
SFbFSCIL [80]	ICCV 2021	61.40	59.80	54.20	51.69	49.45	48.00	45.20	43.80	42.10	50.63	+17.26	
Data-free Replay [6]	ECCV 2022	71.84	67.12	63.21	59.77	57.01	53.95	51.55	49.52	48.21	58.02	+11.15	
LIMIT [18]	TPAMI 2022	72.32	68.47	64.30	60.78	57.95	55.07	52.70	50.72	49.19	59.06	+10.17	
MetaFSCIL [17]	CVPR 2022	72.04	67.94	63.77	60.29	57.58	55.16	52.90	50.79	49.19	58.85	+10.17	
FACT [3]	CVPR 2022	72.56	69.63	66.38	62.77	60.6	57.33	54.34	52.16	50.49	60.70	+8.87	
C-FSCIL [16]	CVPR 2022	76.40	71.14	66.46	63.29	60.42	57.46	54.78	53.11	51.41	61.61	+7.95	
Regularizer [12]	ICLR 2022	80.37	74.68	69.39	65.51	62.38	59.03	56.36	53.95	51.73	63.71	+7.63	
TEEN [87]	NeurIPS 2023	73.53	70.55	66.37	63.23	60.53	57.95	55.24	53.44	52.08	61.44	+7.28	
CABD [88]	CVPR 2023	74.65	70.43	66.29	62.77	60.75	57.24	54.79	53.65	52.22	61.42	+7.14	
ALICE [8]	ECCV 2022	80.60	70.60	67.40	64.50	62.50	60.00	57.80	56.80	55.70	63.99	+3.66	
NC-FSCIL [19]	ICLR 2023	84.02	76.80	72.00	67.83	66.35	64.04	61.46	59.54	58.31	67.82	+1.05	
<i>Dynamic adaptation methods</i>													
TOPIC [1]	CVPR 2020	61.31	50.09	45.17	41.16	37.48	35.52	32.19	29.46	24.42	39.64	+34.94	
LEC-Net [21]	arXiv 2022	61.31	35.37	36.66	38.59	33.90	35.89	36.12	32.97	30.55	37.92	+29.69	
DSN [23]	TPAMI 2022	68.95	63.46	59.78	55.64	52.85	51.23	48.9	46.78	45.89	54.83	+13.47	
CEC [2]	CVPR 2021	72.00	66.83	62.97	59.43	56.70	53.73	51.19	49.24	47.63	57.75	+11.73	
FeSSSS [89]	CVPR 2022	81.50	77.04	72.92	69.56	67.27	64.34	62.07	60.55	58.87	68.23	+0.49	
Mamba-FSCIL (ours)		84.93	80.02	74.61	71.33	69.15	65.62	62.38	60.93	59.36	69.81		

5.1 Implementation Details

Datasets. We employed three benchmark datasets. miniImageNet is a variant of ImageNet with 100 classes, each having 500 training and 100 testing images of 84×84 pixels. CIFAR-100 has the same number of classes and images, and the image size is 32×32 . CUB-200 is a fine-grained classification dataset consisting of 11,788 images in 200 classes, with an image resolution of 224×224 . We followed the standard experimental settings in FSCIL [1], [2], [19]. For miniImageNet and CIFAR-100, the base session includes 60 classes, followed by 8 incremental sessions, each with a 5-way 5-shot setting (5 classes and 5 images per class). For CUB-200, the base session comprises 100 classes, with 10 incremental sessions, each following a 10-way 5-shot setting.

Training Details. We employed the standard data preprocessing and augmentation techniques, including random resizing, flipping, and color jittering [1], [2], [8], [19]. We conducted training with a batch size of 512 for base sessions and 64 for incremental sessions, which includes new session data along with intermediate features stored in memory.

For miniImageNet, we utilized ResNet12 [115] as the backbone and train for 500 epochs in the base session, followed by 100-170 iterations in each incremental session. The initial learning rate is 0.25 for the base session and 0.01 for the incremental sessions.

For CIFAR-100, we utilized ResNet12 [115] as the backbone and trained the base session for 200 epochs, followed by 200 iterations per incremental session. The initial learning rate is 0.25 for both the base and incremental sessions.

For CUB-200, we employed two different architectures. In Table 3, ResNet18 [115] serves as the backbone, where we trained the model for 80 epochs in the base session and then proceeded with 200-290 iterations for each incremen-

tal session. In Table 4, we utilized the Swin Transformer Tiny [30] with an input resolution of 384×384 , we trained the model for 80 epochs during the base session followed by 600 iterations per incremental session. Initial learning rates are set at 0.02 for the backbone and 0.2 for the projector during the base session, and are reduced to 0.05 for the incremental sessions.

We apply a cosine annealing strategy for the learning rate and use SGD with a momentum of 0.009 and a weight decay of 0.0005 as the optimizer. The hyper-parameters α and β are set between 50 and 200, 0.05 and 0.5, respectively. The dimensions of the input-dependent parameters in Eq. (9) are set as $D_B = D_C = D_\Delta = 256$. The dimensions D' in Eq. (6) are set to 512, 512, 1024 for CIFAR-100, CUB-200, and miniImageNet datasets, respectively. All experiments are conducted using 8 NVIDIA A100 GPUs.

Zero Initialization. In our incremental learning process, we fixed the identity branch and selective SSM branch from the base session g^{base} and introduced a new selective SSM branch g^{inc} for the incremental sessions. To prevent disruption of pre-existing feature representations, we applied zero initialization to g^{inc} by setting the projection parameters of f_z for the gating features \mathbf{Z}^{inc} to zero, ensuring that its initial outputs (μ^{inc}) are also zero. This approach ensures that g^{inc} begins without affecting the model’s learned features from the base session. As training progresses, g^{inc} is gradually optimized, allowing the model to adapt to new classes by learning feature shifts while preserving the knowledge acquired during the base session.

5.2 Comparison with the State-of-the-art Methods

The comparison with the state-of-the-art methods on miniImageNet, CIFAR-100, and CUB-200 is shown in Ta-

TABLE 2: FSCIL performance across sessions on CIFAR-100 compared with other methods. "Average Acc." is the average accuracy across all sessions. "Final Improv." denotes the accuracy improvement of our method in the last session compared to previous methods.

Methods	Venue	Accuracy in each session (%) \uparrow										Average	Final
		0	1	2	3	4	5	6	7	8	Acc.	Improv.	
<i>Static adaptation methods</i>													
Self-promoted [86]	CVPR 2021	64.10	65.86	61.36	57.45	53.69	50.75	48.58	45.66	43.25	54.52	+14.26	
Data-free Replay [6]	ECCV 2022	74.40	70.20	66.54	62.51	59.71	56.58	54.52	52.39	50.14	60.78	+7.37	
MetaFSCIL [17]	CVPR 2022	74.50	70.10	66.84	62.77	59.48	56.52	54.36	52.56	49.97	60.79	+7.54	
C-FSCIL [16]	CVPR 2022	77.47	72.40	67.47	63.25	59.84	56.95	54.42	52.47	50.47	61.64	+7.04	
LIMIT [18]	TPAMI 2022	73.81	72.09	67.87	63.89	60.70	57.77	55.67	53.52	51.23	61.84	+6.28	
FACT [3]	CVPR 2022	74.60	72.09	67.56	63.52	61.38	58.36	56.28	54.24	52.10	62.24	+5.41	
TEEN [87]	NeurIPS 2023	74.92	72.65	68.74	65.01	62.01	59.29	57.90	54.76	52.64	63.10	+4.87	
ALICE [8]	ECCV 2022	79.00	70.50	67.10	63.40	61.20	59.20	58.10	56.30	54.10	63.21	+3.41	
CABD [88]	CVPR 2023	79.45	75.38	71.84	67.95	64.96	61.95	60.16	57.67	55.88	66.14	+1.63	
NC-FSCIL [19]	ICLR 2023	82.52	76.82	73.34	69.68	66.19	62.85	60.96	59.02	56.11	67.50	+1.40	
<i>Dynamic adaptation methods</i>													
TOPIC [1]	CVPR 2020	64.10	55.88	47.07	45.16	40.11	36.38	33.96	31.55	29.37	42.62	+28.14	
LEC-Net [21]	arXiv 2022	64.10	53.23	44.19	41.87	38.54	39.54	37.34	34.73	34.73	43.14	+22.78	
CEC [2]	CVPR 2021	73.07	68.88	65.26	61.19	58.09	55.57	53.22	51.34	49.14	59.53	+8.37	
DSN [23]	TPAMI 2022	73.00	68.83	64.82	62.24	59.16	56.96	54.04	51.57	49.35	60.00	+8.16	
FeSSSS [89]	CVPR 2022	75.35	70.81	66.70	62.73	59.62	56.45	54.33	52.10	50.23	60.92	+7.28	
Mamba-FSCIL (ours)		82.80	77.85	73.69	69.67	66.89	63.66	61.48	59.74	57.51	68.14		

TABLE 3: FSCIL performance across sessions on CUB-200 compared with other methods. "Average Acc." is the average accuracy across all sessions. "Final Improv." shows the last session's accuracy improvement of our method over previous methods.

Methods	Venue	Accuracy in each session (%) \uparrow												Average	Final
		0	1	2	3	4	5	6	7	8	9	10	Acc.	Improv.	
<i>Static adaptation methods</i>															
Self-promoted [86]	CVPR 2021	68.68	61.85	57.43	52.68	50.19	46.88	44.65	43.07	40.17	39.63	37.33	49.32	+24.32	
SFbFSCIL [80]	ICCV 2021	68.78	59.37	59.32	54.96	52.58	49.81	48.09	46.32	44.33	43.43	43.23	51.84	+18.42	
Data-free replay [6]	ECCV 2022	75.90	72.14	68.64	63.76	62.58	59.11	57.82	55.89	54.92	53.58	52.39	61.52	+9.26	
MetaFSCIL [17]	CVPR 2022	75.9	72.41	68.78	64.78	62.96	59.99	58.3	56.85	54.78	53.82	52.64	61.93	+9.01	
MgSvF [116]	TPAMI 2021	72.29	70.53	67.00	64.92	62.67	61.89	59.63	59.15	57.73	55.92	54.33	62.37	+7.32	
FACT [3]	CVPR 2022	75.90	73.23	70.84	66.13	65.56	62.15	61.74	59.83	58.41	57.89	56.94	64.42	+4.71	
IDLVQ [11]	ICLR 2021	77.37	74.72	70.28	67.13	65.34	63.52	62.10	61.54	59.04	58.68	57.81	65.23	+3.84	
LIMIT [18]	TPAMI 2022	76.32	74.18	72.68	69.19	68.79	65.64	63.57	62.69	61.47	60.44	58.45	66.67	+3.20	
TEEN [87]	NeurIPS 2023	77.26	76.13	72.81	68.16	67.77	64.40	63.25	62.29	61.19	60.32	59.31	66.63	+2.34	
NC-FSCIL [19]	ICLR 2023	80.45	75.98	72.30	70.28	68.17	65.16	64.43	63.25	60.66	60.01	59.44	67.28	+2.21	
ALICE [8]	ECCV 2022	77.40	72.70	70.60	67.20	65.90	63.40	62.90	61.90	60.50	60.60	60.10	65.75	+1.55	
<i>Dynamic adaptation methods</i>															
TOPIC [1]	CVPR 2020	68.68	62.49	54.81	49.99	45.25	41.40	38.35	35.36	32.22	28.31	26.28	43.92	+35.37	
LEC-Net [21]	arXiv 2022	70.86	58.15	54.83	49.34	45.85	40.55	39.70	34.59	36.58	33.56	31.96	45.08		
CEC [2]	CVPR 2021	75.85	71.94	68.50	63.50	62.43	58.27	57.73	55.81	54.83	53.52	52.28	61.33	+9.37	
FeSSSS [89]	CVPR 2022	79.60	73.46	70.32	66.38	63.97	59.63	58.19	57.56	55.01	54.31	52.98	62.85	+8.67	
DSN [23]	TPAMI 2022	76.06	72.18	69.57	66.68	64.42	62.12	60.16	58.94	56.99	55.10	54.21	63.31	+7.44	
Mamba-FSCIL (ours)		80.90	76.26	72.97	70.14	67.83	65.74	65.43	64.12	62.31	62.12	61.65	68.13		

ble 1, Table 2, and Table 3. The results demonstrate that Mamba-FSCIL consistently outperforms almost all existing static and dynamic adaptation methods by over 1% in terms of last-session accuracy, where all classes are taken into account. Specifically, on miniImageNet, Mamba-FSCIL achieves the highest average accuracy of 69.81% and increases the last-session accuracy to 59.36%, which surpasses the challenging baseline NC-FSCIL [19] by 1.99% and 1.05%, respectively. In CIFAR-100, Mamba-FSCIL maintains the best performance in most sessions, with the accuracy of the last session outperforming NC-FSCIL by 1.4%. Notably,

Mamba-FSCIL significantly surpasses dynamic methods such as FeSSSS [89] with an average accuracy improvement of 7.22% over FeSSSS. In the more challenging fine-grained CUB-200 dataset, Mamba-FSCIL leads with an average accuracy of 68.13%, outperforming all static and dynamic methods. Compared to DSN, Mamba-FSCIL shows the remarkable ability to learn complex classification scenarios incrementally, improving the accuracy in the last session by 7.44%, also indicating a lower performance drop over sessions.

To further test Mamba-FSCIL on larger vision models,

TABLE 4: FSCIL performance across sessions on CUB-200 using Swin Transformer-Tiny backbone. "Average Acc." represents the average accuracy across all sessions. "PD" indicates the performance drop, calculated as the difference in accuracy between the first and last session. Results for CLOM [104] and Comp-FSCIL [83] are taken from Comp-FSCIL [83], while NC-FSCIL [19] results are from our implementation using the same training settings as Mamba-FSCIL for a fair comparison.

Methods	Venue	Accuracy in each session (%) \uparrow											Average Acc.	PD
		0	1	2	3	4	5	6	7	8	9	10		
CLOM [104]	NeurIPS 2022	86.28	82.85	80.61	77.79	76.34	74.64	73.62	72.82	71.24	71.33	70.50	76.18	15.78
NC-FSCIL [19]	ICLR 2023	87.53	84.25	81.72	79.10	77.21	75.52	74.51	74.42	72.26	72.86	72.49	77.44	15.04
Comp-FSCIL [83]	ICML 2024	87.67	84.73	83.03	80.04	77.73	75.52	74.32	74.55	73.35	73.15	72.80	77.90	14.87
Mamba-FSCIL (ours)		88.13	85.14	83.41	80.77	77.23	75.73	75.70	75.32	74.18	74.26	74.13	78.55	14.00

TABLE 5: Ablation study on the impact of dual selective projector and class-sensitive selective scan mechanism on FSCIL performance across different datasets. "BASE" indicates the accuracy in the first session; "FINAL" refers to the last session; "PD" represents the performance drop between the first and last sessions.

Methods	Adaptation Type	miniImageNet			CIFAR-100			CUB-200		
		BASE \uparrow	FINAL \uparrow	PD \downarrow	BASE \uparrow	FINAL \uparrow	PD \downarrow	BASE \uparrow	FINAL \uparrow	PD \downarrow
Baseline	Static	84.02	58.31	25.71	82.52	56.11	26.41	80.45	59.44	21.01
+ Single Selective SSM Projector	Dynamic	84.93	57.89	27.04	82.80	56.07	26.73	80.90	60.70	20.20
+ Dual Selective SSM Projector	Dynamic	84.93	58.92	26.01	82.80	56.71	26.09	80.90	61.06	19.84
+ Dual Selective SSM Projector + Class-sensitive Selective Scan	Dynamic	84.93	59.36	25.57	82.80	57.51	25.29	80.90	61.65	19.25

we evaluated it on the CUB-200 dataset using a Swin Transformer-Tiny [30] backbone pre-trained on ImageNet-1K [117]. We compared it against the state-of-the-art methods using the same backbone, including CLOM [104], NC-FSCIL [19], and Comp-FSCIL [83]. As shown in Table 4, Mamba-FSCIL achieves the highest average session accuracy of 78.55% and the lowest performance drop (PD), reducing PD to 14.00% compared to Comp-FSCIL’s 14.87%. Notably, while Comp-FSCIL leverages human-inspired compositional learning for adaptive concept integration, Mamba-FSCIL, without relying on this extra step, still outperforms Comp-FSCIL, demonstrating the strong potential of our approach.

5.3 Ablation Studies

5.3.1 Impact of Individual Component

We performed ablation studies across the three datasets to assess the impact of our dual selective projector and class-sensitive selective scan mechanism. Utilizing a consistent setup that includes the same backbone, identity branch, memory module, classifier, and classification loss, we explored several configurations: (1) **Baseline** employs NC-FSCIL with a static MLP-based projection layer, serving as a competitive static adaptation method. (2) **+ Single Selective SSM Projector** integrates a single dynamic SSM projector with one projection branch, updated across all sessions. (3) **+ Dual Selective SSM Projector** uses our dual selective SSM projector with two branches, as introduced in Section 4.2. (4) **+ Dual Selective SSM Projector + Class-sensitive Selective Scan** further integrates our class-sensitive selective scan.

The results in Table 5 show that the introduction of a single selective SSM projector improves base session accuracy across the three datasets (e.g., from 84.02% to 84.93% on miniImageNet and from 82.52% to 82.80% on CIFAR-100), demonstrating the Mamba-based projector helps to

improve the performance in the base session, providing a more powerful feature extractor for the subsequent sessions. However, despite these gains, the final performances on miniImageNet and CIFAR-100 both fall below the baseline, implying that a naive replacement of the MLP projector with the selective SSM projector cannot effectively mitigate catastrophic forgetting, increasing the performance drop as a result. In contrast, when our proposed dual selective SSM projector is adopted, the final performance is also effectively improved over the baseline, reducing the performance drop from 27.04% to 26.01% on miniImageNet and from 26.73% to 26.09% on CIFAR-100. This shows that our dual design is capable of adaptively learning feature shifts of novel classes into their corresponding classifier prototypes with fewer disruptions to the learned knowledge of the base classes. Further improvements are achieved with the integration of our class-sensitive scan mechanism into the dual projector, increasing the last-session accuracy from 56.71% to 57.51% on CIFAR-100 and from 61.06% to 61.65% on CUB-200. These findings validate the critical role of each component in Mamba-FSCIL.

5.3.2 Impact of Losses in Class-sensitive Selective Scan

We investigated the impacts of the suppression and separation losses introduced in Section 4.3 by analyzing the features extracted from the test set of the miniImageNet. First, we measured the average cosine similarity between the final representations and the classifier prototypes across all base classes in Fig. 3, defined as:

$$\frac{1}{\sum_{k=1}^K N_k} \sum_{k=1}^K \sum_{i=1}^{N_k} \cos(\boldsymbol{\mu}_{k,i}, \mathbf{w}_k), \quad (23)$$

where $\boldsymbol{\mu}_{k,i}$ represents the feature vector of sample i in class k , N_k is the number of samples in class k , \mathbf{w}_k is the classifier prototype for class k , and K is the number of base classes.

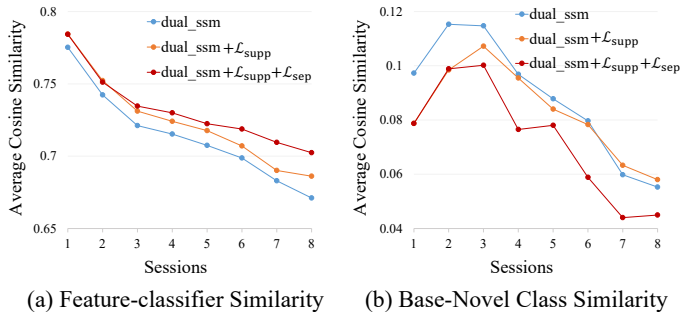


Fig. 3: Effect of suppression and separation losses in Class-sensitive Selective Scan mechanism on feature-classifier alignment and base-novel class separability in the miniImageNet test set: (a) Average cosine similarity between base-class features and their corresponding classifiers; (b) Average cosine similarity between base and novel classes.

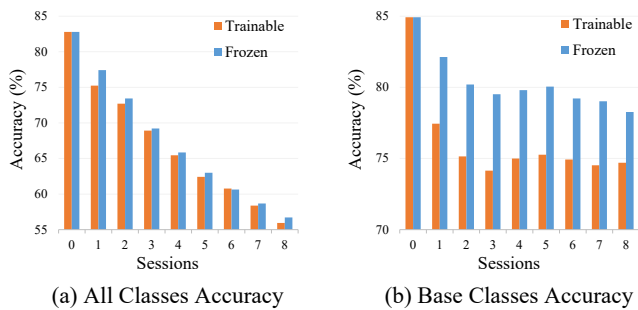


Fig. 4: Impact of freezing vs. training the identity branch p and the selective SSM branch g^{base} during incremental sessions on miniImageNet: (a) Accuracy for all classes, (b) Accuracy for base classes.

To assess the separability between base and novel classes, we calculated the average cosine similarity for any possible pairing of base and novel classes feature vectors as:

$$\frac{1}{N_{\text{base}}N_{\text{novel}}} \sum_{i=1}^{N_{\text{base}}} \sum_{j=1}^{N_{\text{novel}}} \cos\langle \boldsymbol{\mu}_{\text{base},i}, \boldsymbol{\mu}_{\text{novel},j} \rangle, \quad (24)$$

where $\boldsymbol{\mu}_{\text{base},i}$ and $\boldsymbol{\mu}_{\text{novel},j}$ are feature vectors of the i -th base class sample and j -th novel class sample, respectively. The terms N_{base} and N_{novel} denote the total number of samples in base and novel classes in the test set of miniImageNet.

Fig. 3 (a) shows that the incorporation of suppression loss $\mathcal{L}_{\text{supp}}$ helps to improve base-class alignment between features and classifier prototypes in late sessions, facilitating the maintenance of base-class performance. When the separation loss \mathcal{L}_{sep} is further added, as shown in Fig. 3 (b), the similarities of features between the base-class and novel-class are significantly reduced, which leaves sufficient feature space for incremental training sessions and boosts the novel-class accuracy.

5.3.3 Effect of Freezing vs. Training Projection Branches

We assessed the impact of freezing the identity branch p and the selective SSM branch g^{base} from the base session during incremental learning. Models are trained on the miniImageNet dataset, utilizing a ResNet-12 backbone. Two

TABLE 6: Impact of hyper-parameters α and β on performance in the miniImageNet dataset. ‘‘Average Acc.’’ represents the average accuracy across all sessions.

Impact of hyper-parameter α					
Value	40	80	120	140	160
Average Acc.	69.72	69.81	69.81	69.80	69.79
Impact of hyper-parameter β					
Value	0.05	0.1	0.3	0.5	0.7
Average Acc.	69.64	69.70	69.71	69.81	69.79

TABLE 7: Impact of the number of scan paths (K) on model performance for CIFAR-100 and CUB-200 datasets. ‘‘BASE’’ refers to accuracy in the first session; ‘‘FINAL’’ to the accuracy in the last session; and ‘‘AVG’’ to the average accuracy across all sessions.

K	CIFAR-100			CUB-200		
	BASE \uparrow	FINAL \uparrow	AVG \uparrow	BASE \uparrow	FINAL \uparrow	AVG \uparrow
1	82.35	55.94	67.23	80.41	60.84	67.48
2	82.65	57.13	67.53	80.49	61.08	67.86
4	82.80	57.51	68.14	80.90	61.65	68.13

configurations are compared: one with p and g^{base} frozen (as described in Section 4.2) and the other one with them trainable throughout the incremental sessions. The results in Fig. 4 indicate that the frozen configuration achieves higher accuracy across all classes (Fig. 4 (a)) and specifically for base classes (Fig. 4 (b)) in most sessions. This result implies that freezing p and g^{base} effectively preserves the base-session knowledge, mitigating catastrophic forgetting.

5.3.4 Sensitivity Analysis of Hyper-parameters α and β

We conducted a sensitivity analysis on the hyper-parameters α and β of Eq. (22) in Table 6 to evaluate their impact on our model’s average accuracy on miniImageNet. Each experiment varies one parameter with the other fixed. The results show that when α and β are set within a proper range, the performance only varies slightly, demonstrating the model’s robustness to the hyper-parameters.

5.3.5 Impact of the Number of Training Samples

We explored the effect of varying the number of training samples per class, or ‘‘shots,’’ on Mamba-FSCIL’s performance. As shown in Fig. 5, increasing the number of training examples from 1-shot to 20-shot consistently improves accuracy across all sessions for the miniImageNet, CIFAR-100, and CUB-200 datasets. This demonstrates that Mamba-FSCIL benefits from the additional novel class training samples while effectively preserving base class knowledge, and preventing catastrophic forgetting.

5.3.6 Impact of the Number of Scan Paths

We evaluated the influence of varying the number of scan paths (K) on Mamba-FSCIL’s performance on CIFAR-100 and CUB-200 datasets, as described in Table 7. Increasing the scan paths consistently enhances all performance metrics—base, final, and average session accuracies. Specifically,

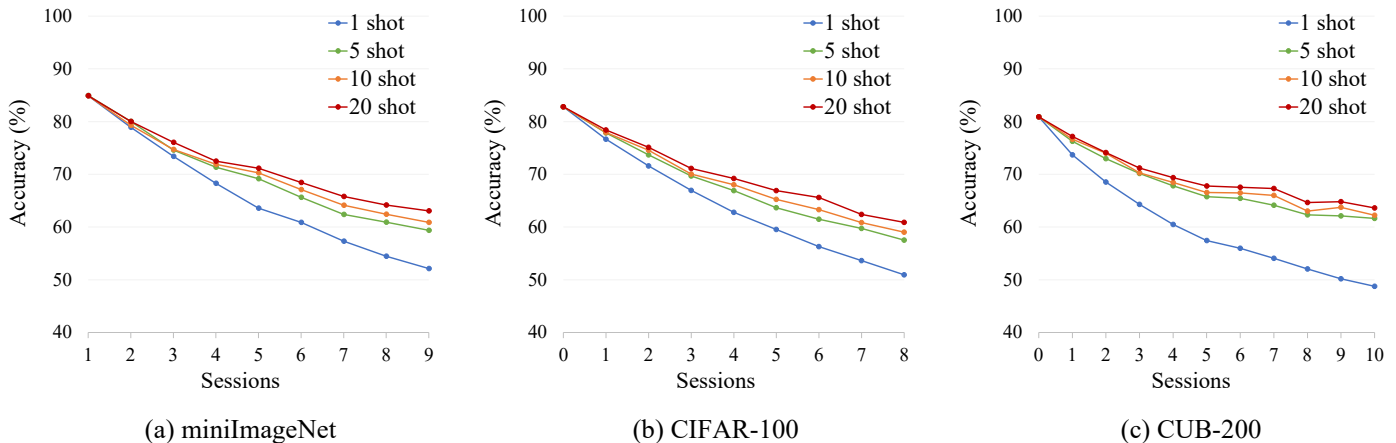


Fig. 5: Performance across different sessions for 1-shot, 5-shot, 10-shot, and 20-shot learning scenarios on miniImageNet, CIFAR-100, and CUB-200 datasets.

TABLE 8: Performance comparison of different projection architectures on CIFAR-100.

Projector Architecture	BASE \uparrow	FINAL \uparrow	AVG \uparrow
Dual Transformer	82.45	55.05	66.46
Dual MLP	82.57	56.02	67.57
Dual Selective SSM (ours)	82.80	57.24	68.08

on CIFAR-100, elevating the scan paths from 1 (top-left to bottom-right) to 2 (adding bottom-right to top-left) boosts final session accuracy by 1.19%, from 55.94% to 57.13%, increases base session accuracy from 82.35% to 82.65%, and raises average accuracy from 67.23% to 67.53%. Extending to four paths (adding top-right to bottom-left and bottom-left to top-right) further improves final session accuracy to 57.51%, base session accuracy to 82.80%, and average accuracy to 68.14%. Observations on CUB-200 reflect similar trends. These findings highlight the substantial benefits of more scan paths in improving model performance, particularly their role in enhancing the integration of contextual information from multiple directions, which is crucial for handling complex visual tasks in dynamic learning environments. By default, we employed four scan paths in all experiments.

5.4 Comparison with Different Projection Architectures

To validate the effectiveness of the selective SSM projection branches in the Dual Selective SSM Projector for FSCIL, we performed a comparative experiment on the CIFAR-100 dataset. In this experiment, we replaced the selective SSM branches in our dual-branch architecture with MLP and Transformer structures while maintaining similar parameter counts across all models using a ResNet-12 backbone. The MLP setup includes three layers of multi-layer perceptrons, while the Transformer configuration incorporates a multi-head attention mechanism with 8 heads followed by a feed-forward network. Suppression loss with $\alpha = 50$ is applied across all configurations and is directly applied to the output of the newly attached branch (g^{inc}) in the MLP and Transformer-based setups.

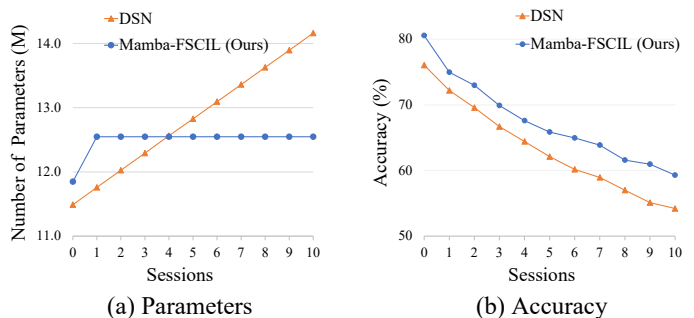


Fig. 6: Comparison of parameter growth (a) and session-wise accuracy (b) between Mamba-FSCIL and DSN [23].

As shown in Table 8, the Dual Selective SSM architecture consistently outperforms both MLP and Transformer setups across all critical metrics: base accuracy, final session accuracy, and average accuracy. Specifically, the Dual Selective SSM architecture enhances final session accuracy by 2.19% compared to the Transformer result and by 1.22% compared to the MLP setup. Furthermore, it achieves an average accuracy improvement of 1.62% over the Transformer and 0.51% over MLP.

5.5 Comparison with Dynamic Adaptation Method

We compared our Mamba-FSCIL with DSN [23] in Fig. 6, particularly in terms of parameter efficiency and session-wise performance. Both methods use the same ResNet18 backbone. As shown in Fig. 6 (a), Unlike DSN, which continually increases its parameter amount to learn new classes, Mamba-FSCIL armed with a dual selective SSM projector dynamically adjusts its parameters without expanding the parameter space. In addition, Fig. 6 (b) illustrates that Mamba-FSCIL consistently outperforms DSN in all sessions, demonstrating Mamba-FSCIL’s superior ability to retain old knowledge while learning new classes.

5.6 Visualization of Activation Maps

We used GradCAM [118] to visualize the activation maps of a Swin Transformer-Tiny model trained on the CUB-200

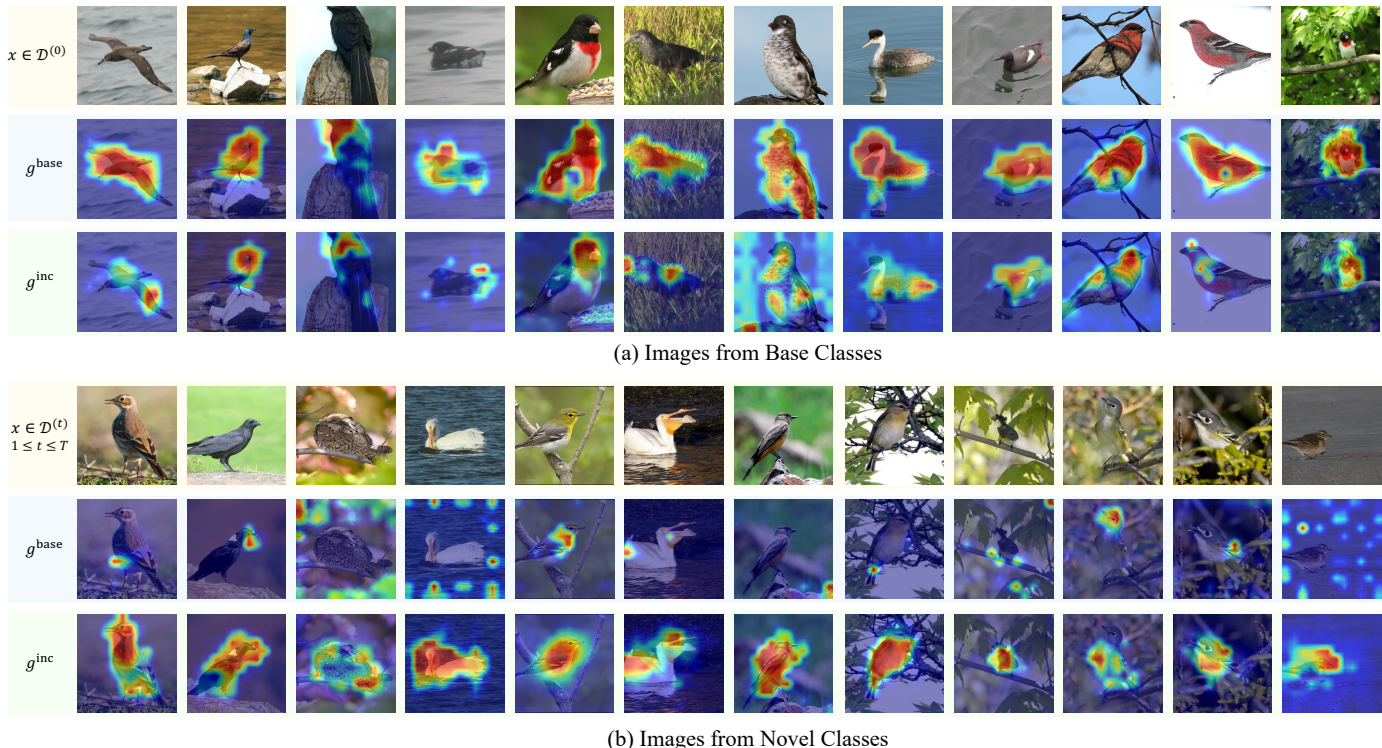


Fig. 7: Activation maps for base and novel classes on the CUB-200 dataset. (a) Base classes; (b) Novel classes. Activation maps are generated using GradCAM from the g^{base} and g^{inc} branches.

dataset after 10 incremental sessions. The activation maps from the g^{base} and g^{inc} branches are visualized to assess their roles in handling base and novel classes.

Fig. 7 (a) shows that for images from the base classes, the g^{base} branch significantly influences the final output, with activation regions effectively covering the main subject, indicating that this branch, fixed during incremental training, retains a strong representation of base classes. This confirms its role in preserving learned knowledge. In contrast, the g^{inc} branch shows minimal activation, reducing interference with established knowledge. For novel classes, as shown in Fig. 7 (b), the fixed g^{base} branch struggles to represent novel classes adequately, with incomplete activation coverage that could lead to classification errors. However, the g^{inc} branch compensates by fully covering the subject, enhancing the model’s ability to represent novel classes. These visualizations demonstrate that the g^{base} branch effectively preserves knowledge from base classes, while the g^{inc} branch improves representation for novel classes without disrupting existing knowledge.

5.7 Analysis of Feature Embeddings

We analyzed feature embeddings using t-SNE visualizations for both base and novel classes from the test set of the CIFAR-100 dataset, comparing the strong baseline NC-FSCIL with our Mamba-FSCIL. Fig. 8 (a) and Fig. 8 (b) show the results of some base classes during the first and last sessions. It is shown that the base-class features of the baseline method are much scattered in the last session. As a comparison, Mamba-FSCIL demonstrates consistent intra-class compactness and distinct inter-class separation, indicating enhanced stability for base classes that better main-

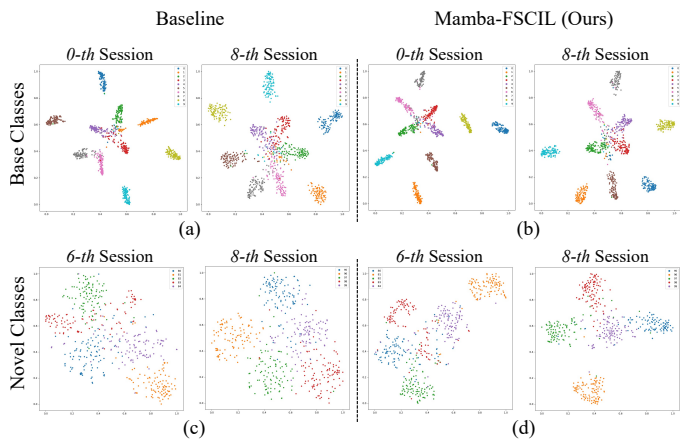


Fig. 8: t-SNE visualization of feature embeddings from the CIFAR-100 dataset, showcasing base classes in (a) and (b) and novel classes in (c) and (d). Each color denotes a different class.

tain their performance in incremental training. Fig. 8 (c) and Fig. 8 (d) depict the results of some novel classes in the 6-th and 8-th sessions. In both sessions, Mamba-FSCIL shows significantly more compact clusters with clearer margins among classes, highlighting its capacity to accommodate new classes. These results explain Mamba-FSCIL’s superior performance in the benchmarks.

6 CONCLUSION AND FUTURE WORKS

In this study, we propose the Mamba-FSCIL framework, leveraging selective state space models to address the challenges of FSCIL. Mamba-FSCIL utilizes a dual selective SSM

projector to achieve dynamic adaptation without the need to continually expand the parameter space of the model. The dual design dynamically adjusts its parameters to integrate new classes while preserving the integrity of previously learned information. Furthermore, the incorporation of the class-sensitive selective scan mechanism, composed of the suppression loss and the separation loss, guides the dynamic adaptation process deliberately, enhancing both stability and adaptability in incremental sessions' training. Empirical results demonstrate that Mamba-FSCIL outperforms the state-of-the-art static and dynamic methods across three benchmark datasets.

Future work for Mamba-FSCIL involves extending it to address highly correlated tasks like online class-incremental and cross-domain incremental learning. We also aim to adapt Mamba-FSCIL for multimodal scenarios, enhancing its effectiveness in dynamic and interactive environments. Additionally, exploring its application in embodied intelligence is also a key direction for future research.

REFERENCES

- [1] X. Tao, X. Hong, X. Chang, S. Dong, X. Wei, and Y. Gong, "Few-shot class-incremental learning," in *Proceedings of the IEEE Conference on Computer Vision and Pattern Recognition*. IEEE, 2020, pp. 12 183–12 192.
- [2] C. Zhang, N. Song, G. Lin, Y. Zheng, P. Pan, and Y. Xu, "Few-shot incremental learning with continually evolved classifiers," in *Proceedings of the IEEE Conference on Computer Vision and Pattern Recognition*. IEEE, 2021, pp. 12 455–12 464.
- [3] D.-W. Zhou, F.-Y. Wang, H.-J. Ye, L. Ma, S. Pu, and D.-C. Zhan, "Forward compatible few-shot class-incremental learning," in *Proceedings of the IEEE Conference on Computer Vision and Pattern Recognition*. IEEE, 2022, pp. 9046–9056.
- [4] J. Zhang, L. Liu, O. Silven, M. Pietikäinen, and D. Hu, "Few-shot class-incremental learning: A survey," *arXiv preprint arXiv:2308.06764*, 2023.
- [5] S. Tian, L. Li, W. Li, H. Ran, X. Ning, and P. Tiwari, "A survey on few-shot class-incremental learning," *Neural Networks*, vol. 169, pp. 307–324, 2024.
- [6] H. Liu, L. Gu, Z. Chi, Y. Wang, Y. Yu, J. Chen, and J. Tang, "Few-shot class-incremental learning via entropy-regularized data-free replay," in *Proceedings of the European Conference on Computer Vision*. Springer, 2022, pp. 146–162.
- [7] A. Agarwal, B. Banerjee, F. Cuzzolin, and S. Chaudhuri, "Semantics-driven generative replay for few-shot class incremental learning," in *Proceedings of the International ACM Conference on Multimedia*. ACM, 2022, pp. 5246–5254.
- [8] C. Peng, K. Zhao, T. Wang, M. Li, and B. C. Lovell, "Few-shot class-incremental learning from an open-set perspective," in *Proceedings of the European Conference on Computer Vision*. Springer, 2022, pp. 382–397.
- [9] X. Tao, X. Chang, X. Hong, X. Wei, and Y. Gong, "Topology-preserving class-incremental learning," in *Proceedings of the European Conference on Computer Vision*. Springer, 2020, pp. 254–270.
- [10] A. Cheraghian, S. Rahman, P. Fang, S. K. Roy, L. Petersson, and M. Harandi, "Semantic-aware knowledge distillation for few-shot class-incremental learning," in *Proceedings of the IEEE Conference on Computer Vision and Pattern Recognition*. IEEE, 2021, pp. 2534–2543.
- [11] K. Chen and C.-G. Lee, "Incremental few-shot learning via vector quantization in deep embedded space," in *Proceedings of the International Conference on Learning Representations*, 2021.
- [12] A. F. Akyürek, E. Akyürek, D. Wijaya, and J. Andreas, "Subspace regularizers for few-shot class incremental learning," in *International Conference on Learning Representations*, 2022.
- [13] S. Dong, X. Hong, X. Tao, X. Chang, X. Wei, and Y. Gong, "Few-shot class-incremental learning via relation knowledge distillation," in *Proceedings of the AAAI Conference on Artificial Intelligence*. AAAI, 2021, pp. 1255–1263.
- [14] K. Joseph, S. Khan, F. S. Khan, R. M. Anwer, and V. N. Balasubramanian, "Energy-based latent aligner for incremental learning," in *Proceedings of the IEEE Conference on Computer Vision and Pattern Recognition*. IEEE, 2022, pp. 7452–7461.
- [15] B. Lu, X. Gan, L. Yang, W. Zhang, L. Fu, and X. Wang, "Geometer: Graph few-shot class-incremental learning via prototype representation," in *Proceedings of the ACM SIGKDD Conference on Knowledge Discovery and Data Mining*. ACM, 2022, pp. 1152–1161.
- [16] M. Hersche, G. Karunaratne, G. Cherubini, L. Benini, A. Sebastian, and A. Rahimi, "Constrained few-shot class-incremental learning," in *Proceedings of the IEEE Conference on Computer Vision and Pattern Recognition*. IEEE, 2022, pp. 9057–9067.
- [17] Z. Chi, L. Gu, H. Liu, Y. Wang, Y. Yu, and J. Tang, "Meta-fscil: A meta-learning approach for few-shot class incremental learning," in *Proceedings of the IEEE Conference on Computer Vision and Pattern Recognition*. IEEE, 2022, pp. 14 166–14 175.
- [18] D.-W. Zhou, H.-J. Ye, L. Ma, D. Xie, S. Pu, and D.-C. Zhan, "Few-shot class-incremental learning by sampling multi-phase tasks," *IEEE Transactions on Pattern Analysis and Machine Intelligence*, vol. 45, no. 11, pp. 12 816–12 831, 2022.
- [19] Y. Yang, H. Yuan, X. Li, Z. Lin, P. Torr, and D. Tao, "Neural collapse inspired feature-classifier alignment for few-shot class-incremental learning," in *Proceedings of the International Conference on Learning Representations*, 2023.
- [20] S. W. Yoon, D.-Y. Kim, J. Seo, and J. Moon, "Xtarnet: Learning to extract task-adaptive representation for incremental few-shot learning," in *Proceedings of the International Conference on Machine Learning*. PMLR, 2020, pp. 10 852–10 860.
- [21] B. Yang, M. Lin, B. Liu, M. Fu, C. Liu, R. Ji, and Q. Ye, "Learnable expansion-and-compression network for few-shot class-incremental learning," *arXiv preprint arXiv:2104.02281*, 2021.
- [22] S. Yan, J. Xie, and X. He, "Der: Dynamically expandable representation for class incremental learning," in *Proceedings of the IEEE Conference on Computer Vision and Pattern Recognition*. IEEE, 2021, pp. 3014–3023.
- [23] B. Yang, M. Lin, Y. Zhang, B. Liu, X. Liang, R. Ji, and Q. Ye, "Dynamic support network for few-shot class incremental learning," *IEEE Transactions on Pattern Analysis and Machine Intelligence*, vol. 45, no. 3, pp. 2945–2951, 2022.
- [24] F.-Y. Wang, D.-W. Zhou, H.-J. Ye, and D.-C. Zhan, "Foster: Feature boosting and compression for class-incremental learning," in *Proceedings of the European Conference on Computer Vision*. Springer, 2022, pp. 398–414.
- [25] A. Douillard, A. Ramé, G. Couairon, and M. Cord, "Dytox: Transformers for continual learning with dynamic token expansion," in *Proceedings of the IEEE Conference on Computer Vision and Pattern Recognition*. IEEE, 2022, pp. 9285–9295.
- [26] Z. Li, C. Zhong, S. Liu, R. Wang, and W.-S. Zheng, "Preserving earlier knowledge in continual learning with the help of all previous feature extractors," *arXiv preprint arXiv:2104.13614*, 2021.
- [27] A. Gu and T. Dao, "Mamba: Linear-time sequence modeling with selective state spaces," *arXiv preprint arXiv:2312.00752*, 2023.
- [28] A. Vaswani, N. Shazeer, N. Parmar, J. Uszkoreit, L. Jones, A. N. Gomez, Ł. Kaiser, and I. Polosukhin, "Attention is all you need," in *Proceedings of the Advances in Neural Information Processing Systems*. MIT Press, 2017.
- [29] A. Dosovitskiy, L. Beyer, A. Kolesnikov, D. Weissenborn, X. Zhai, T. Unterthiner, M. Dehghani, M. Minderer, G. Heigold, S. Gelly *et al.*, "An image is worth 16x16 words: Transformers for image recognition at scale," in *Proceedings of the International Conference on Learning Representations*, 2020.
- [30] Z. Liu, Y. Lin, Y. Cao, H. Hu, Y. Wei, Z. Zhang, S. Lin, and B. Guo, "Swin transformer: Hierarchical vision transformer using shifted windows," in *Proceedings of the IEEE International Conference on Computer Vision*. IEEE, 2021, pp. 10 012–10 022.
- [31] Y. Liu, Y. Tian, Y. Zhao, H. Yu, L. Xie, Y. Wang, Q. Ye, and Y. Liu, "Vmamba: Visual state space model," *arXiv preprint arXiv:2401.10166*, 2024.
- [32] T. Chen, Z. Tan, T. Gong, Q. Chu, Y. Wu, B. Liu, J. Ye, and N. Yu, "Mim-istd: Mamba-in-mamba for efficient infrared small target detection," *arXiv preprint arXiv:2403.02148*, 2024.
- [33] J. Ruan and S. Xiang, "Vm-unet: Vision mamba unet for medical image segmentation," *arXiv preprint arXiv:2402.02491*, 2024.
- [34] J. Liu, H. Yang, H.-Y. Zhou, Y. Xi, L. Yu, Y. Yu, Y. Liang, G. Shi, S. Zhang, H. Zheng *et al.*, "Swin-umamba: Mamba-based unet with imagenet-based pretraining," *arXiv preprint arXiv:2402.03302*, 2024.

- [35] L. Zhu, B. Liao, Q. Zhang, X. Wang, W. Liu, and X. Wang, "Vision mamba: Efficient visual representation learning with bidirectional state space model," in *Proceedings of the International Conference on Machine Learning*. PMLR, 2024.
- [36] K. Li, X. Li, Y. Wang, Y. He, Y. Wang, L. Wang, and Y. Qiao, "Videomamba: State space model for efficient video understanding," *arXiv preprint arXiv:2403.06977*, 2024.
- [37] Z. Xing, T. Ye, Y. Yang, G. Liu, and L. Zhu, "Segmamba: Long-range sequential modeling mamba for 3d medical image segmentation," *arXiv preprint arXiv:2401.13560*, 2024.
- [38] J. Ma, F. Li, and B. Wang, "U-mamba: Enhancing long-range dependency for biomedical image segmentation," *arXiv preprint arXiv:2401.04722*, 2024.
- [39] D. Han, Z. Wang, Z. Xia, Y. Han, Y. Pu, C. Ge, J. Song, S. Song, B. Zheng, and G. Huang, "Demystify mamba in vision: A linear attention perspective," *arXiv preprint arXiv:2405.16605*, 2024.
- [40] S. Ravi and H. Larochelle, "Optimization as a model for few-shot learning," in *Proceedings of the International Conference on Learning Representations*, 2017.
- [41] W.-Y. Chen, Y.-C. Liu, Z. Kira, Y.-C. F. Wang, and J.-B. Huang, "A closer look at few-shot classification," in *Proceedings of the International Conference on Learning Representations*, 2019.
- [42] H.-J. Ye, D.-C. Zhan, Y. Jiang, and Z.-H. Zhou, "Heterogeneous few-shot model rectification with semantic mapping," *IEEE Transactions on Pattern Analysis and Machine Intelligence*, vol. 43, no. 11, pp. 3878–3891, 2020.
- [43] Y. Wang, Q. Yao, J. T. Kwok, and L. M. Ni, "Generalizing from a few examples: A survey on few-shot learning," *ACM computing surveys*, vol. 53, no. 3, pp. 1–34, 2020.
- [44] S. Jadon and A. Jadon, "An overview of deep learning architectures in few-shot learning domain," *arXiv preprint arXiv:2008.06365*, 2020.
- [45] C. Kong, J. Kim, D. Han, and N. Kwak, "Few-shot image generation with mixup-based distance learning," in *Proceedings of the European Conference on Computer Vision*. Springer, 2022, pp. 563–580.
- [46] G. Koch, R. Zemel, R. Salakhutdinov *et al.*, "Siamese neural networks for one-shot image recognition," in *Proceedings of the International Conference on Machine Learning Deep Learning Workshop*. PMLR, 2015, pp. 1–30.
- [47] O. Vinyals, C. Blundell, T. Lillicrap, and D. Wierstra, "Matching networks for one shot learning," in *Proceedings of the Advances in Neural Information Processing Systems*. MIT Press, 2016.
- [48] J. Snell, K. Swersky, and R. Zemel, "Prototypical networks for few-shot learning," in *Proceedings of the Advances in Neural Information Processing Systems*. MIT Press, 2017.
- [49] A. Santoro, S. Bartunov, M. Botvinick, D. Wierstra, and T. Lillicrap, "Meta-learning with memory-augmented neural networks," in *Proceedings of the International Conference on Machine Learning*. PMLR, 2016, pp. 1842–1850.
- [50] T. Munkhdalai and H. Yu, "Meta networks," in *Proceedings of the International Conference on Machine Learning*. PMLR, 2017, pp. 2554–2563.
- [51] C. Finn, P. Abbeel, and S. Levine, "Model-agnostic meta-learning for fast adaptation of deep networks," in *Proceedings of the International Conference on Machine Learning*. PMLR, 2017, pp. 1126–1135.
- [52] A. Nichol, J. Achiam, and J. Schulman, "On first-order meta-learning algorithms," *arXiv preprint arXiv:1803.02999*, 2018.
- [53] G. Cauwenberghs and T. Poggio, "Incremental and decremental support vector machine learning," in *Proceedings of the Advances in Neural Information Processing Systems*. MIT Press, 2000.
- [54] Z. Li and D. Hoiem, "Learning without forgetting," *IEEE Transactions on Pattern Analysis and Machine Intelligence*, vol. 40, no. 12, pp. 2935–2947, 2017.
- [55] S.-A. Rebuffi, A. Kolesnikov, G. Sperl, and C. H. Lampert, "icarl: Incremental classifier and representation learning," in *Proceedings of the IEEE Conference on Computer Vision and Pattern Recognition*. IEEE, 2017, pp. 2001–2010.
- [56] M. Delange, R. Aljundi, M. Masana, S. Parisot, X. Jia, A. Leonardis, G. Slabaugh, and T. Tuytelaars, "A continual learning survey: Defying forgetting in classification tasks," *IEEE Transactions on Pattern Analysis and Machine Intelligence*, 2021.
- [57] M. Masana, X. Liu, B. Twardowski, M. Menta, A. D. Bagdanov, and J. van de Weijer, "Class-incremental learning: survey and performance evaluation on image classification," *arXiv preprint arXiv:2010.15277*, 2020.
- [58] D.-W. Zhou, Q.-W. Wang, Z.-H. Qi, H.-J. Ye, D.-C. Zhan, and Z. Liu, "Class-incremental learning: A survey," *IEEE Transactions on Pattern Analysis and Machine Intelligence*, 2024.
- [59] J. Kirkpatrick, R. Pascanu, N. Rabinowitz, J. Veness, G. Desjardins, A. A. Rusu, K. Milan, J. Quan, T. Ramalho, A. Grabska-Barwinski *et al.*, "Overcoming catastrophic forgetting in neural networks," *Proceedings of the National Academy of Sciences*, vol. 114, no. 13, pp. 3521–3526, 2017.
- [60] R. Aljundi, F. Babiloni, M. Elhoseiny, M. Rohrbach, and T. Tuytelaars, "Memory aware synapses: Learning what (not) to forget," in *Proceedings of the European Conference on Computer Vision*. Springer, 2018, pp. 139–154.
- [61] F. Zenke, B. Poole, and S. Ganguli, "Continual learning through synaptic intelligence," in *Proceedings of the International Conference on Machine Learning*. PMLR, 2017, pp. 3987–3995.
- [62] J. Xu and Z. Zhu, "Reinforced continual learning," in *Proceedings of the Advances in Neural Information Processing Systems*. MIT Press, 2018, pp. 899–908.
- [63] J. Yoon, E. Yang, J. Lee, and S. J. Hwang, "Lifelong learning with dynamically expandable networks," in *Proceedings of the International Conference on Learning Representations*, 2018.
- [64] Y. Wu, Y. Chen, L. Wang, Y. Ye, Z. Liu, Y. Guo, and Y. Fu, "Large scale incremental learning," in *Proceedings of the IEEE Conference on Computer Vision and Pattern Recognition*. IEEE, 2019, pp. 374–382.
- [65] D. Lopez-Paz and M. Ranzato, "Gradient episodic memory for continual learning," in *Proceedings of the Advances in Neural Information Processing Systems*. MIT Press, 2017, pp. 6467–6476.
- [66] A. Chaudhry, M. Ranzato, M. Rohrbach, and M. Elhoseiny, "Efficient lifelong learning with a-gem," in *Proceedings of the International Conference on Learning Representations*, 2018.
- [67] A. Iscen, J. Zhang, S. Lazebnik, and C. Schmid, "Memory-efficient incremental learning through feature adaptation," in *Proceedings of the European Conference on Computer Vision*. Springer, 2020, pp. 699–715.
- [68] Y. Xiang, Y. Fu, P. Ji, and H. Huang, "Incremental learning using conditional adversarial networks," in *Proceedings of the IEEE International Conference on Computer Vision*. IEEE, 2019, pp. 6619–6628.
- [69] E. Belouadah and A. Popescu, "I12m: Class incremental learning with dual memory," in *Proceedings of the IEEE International Conference on Computer Vision*. IEEE, 2019, pp. 583–592.
- [70] S. Hou, X. Pan, C. C. Loy, Z. Wang, and D. Lin, "Learning a unified classifier incrementally via rebalancing," in *Proceedings of the IEEE Conference on Computer Vision and Pattern Recognition*. IEEE, 2019, pp. 831–839.
- [71] J. Rajasegaran, S. Khan, M. Hayat, F. S. Khan, and M. Shah, "itam: An incremental task-agnostic meta-learning approach," in *Proceedings of the IEEE Conference on Computer Vision and Pattern Recognition*. IEEE, 2020, pp. 13 588–13 597.
- [72] B. Zhao, X. Xiao, G. Gan, B. Zhang, and S.-T. Xia, "Maintaining discrimination and fairness in class incremental learning," in *Proceedings of the IEEE Conference on Computer Vision and Pattern Recognition*. IEEE, 2020, pp. 13 208–13 217.
- [73] M. McCloskey and N. J. Cohen, *Catastrophic interference in connectionist networks: The sequential learning problem*, ser. Psychology of Learning and Motivation. Elsevier, 1989, vol. 24.
- [74] I. J. Goodfellow, M. Mirza, D. Xiao, A. Courville, and Y. Bengio, "An empirical investigation of catastrophic forgetting in gradient-based neural networks," *arXiv preprint arXiv:1312.6211*, 2013.
- [75] Y. Yang, X. Li, Z. Zhou, S. L. Song, J. Wu, L. Nie, and B. Ghanem, "Corda: Context-oriented decomposition adaptation of large language models," *arXiv preprint arXiv:2406.05223*, 2024.
- [76] F. Sung, Y. Yang, L. Zhang, T. Xiang, P. H. S. Torr, and T. M. Hospedales, "Learning to compare: Relation network for few-shot learning," in *Proceedings of the IEEE Conference on Computer Vision and Pattern Recognition*. IEEE, 2018, pp. 1199–1208.
- [77] D. O. Hebb, *The organization of behavior: A neuropsychological theory*. Psychology press, 2005.
- [78] S. T. Grossberg, *Studies of mind and brain: Neural principles of learning, perception, development, cognition, and motor control*. Springer Science & Business Media, 2012, vol. 70.
- [79] M. Mermillod, A. Bugaiska, and P. Bonin, "The stability-plasticity dilemma: Investigating the continuum from catastrophic forgetting to age-limited learning effects," p. 504, 2013.

- [80] A. Cheraghian, S. Rahman, S. Ramasinghe, P. Fang, C. Simon, L. Petersson, and M. Harandi, "Synthesized feature based few-shot class-incremental learning on a mixture of subspaces," in *Proceedings of the IEEE International Conference on Computer Vision*. IEEE, 2021, pp. 8661–8670.
- [81] Z. Song, Y. Zhao, Y. Shi, P. Peng, L. Yuan, and Y. Tian, "Learning with fantasy: Semantic-aware virtual contrastive constraint for few-shot class-incremental learning," in *Proceedings of the IEEE Conference on Computer Vision and Pattern Recognition*. IEEE, 2023, pp. 24 183–24 192.
- [82] N. Ahmed, A. Kukleva, and B. Schiele, "Orco: Towards better generalization via orthogonality and contrast for few-shot class-incremental learning," in *Proceedings of the IEEE Conference on Computer Vision and Pattern Recognition*. IEEE, 2024, pp. 28 762–28 771.
- [83] Y. Zou, S. Zhang, Y. Li, R. Li *et al.*, "Compositional few-shot class-incremental learning," in *Proceedings of the International Conference on Machine Learning*. PMLR, 2024.
- [84] D. Goswami, B. Twardowski, and J. Van De Weijer, "Calibrating higher-order statistics for few-shot class-incremental learning with pre-trained vision transformers," in *Proceedings of the IEEE Conference on Computer Vision and Pattern Recognition*. IEEE, 2024, pp. 4075–4084.
- [85] Y. Yang, H. Yuan, X. Li, J. Wu, L. Zhang, Z. Lin, P. Torr, D. Tao, and B. Ghanem, "Neural collapse terminus: A unified solution for class incremental learning and its variants," *arXiv preprint arXiv:2308.01746*, 2023.
- [86] K. Zhu, Y. Cao, W. Zhai, J. Cheng, and Z.-J. Zha, "Self-promoted prototype refinement for few-shot class-incremental learning," in *Proceedings of the IEEE Conference on Computer Vision and Pattern Recognition*. IEEE, 2021, pp. 6801–6810.
- [87] Q.-W. Wang, D.-W. Zhou, Y.-K. Zhang, D.-C. Zhan, and H.-J. Ye, "Few-shot class-incremental learning via training-free prototype calibration," in *Proceedings of the Advances in Neural Information Processing Systems*. MIT Press, 2024.
- [88] L. Zhao, J. Lu, Y. Xu, Z. Cheng, D. Guo, Y. Niu, and X. Fang, "Few-shot class-incremental learning via class-aware bilateral distillation," in *Proceedings of the IEEE Conference on Computer Vision and Pattern Recognition*. IEEE, 2023, pp. 11 838–11 847.
- [89] T. Ahmad, A. R. Dhamija, S. Cruz, R. Rabinowitz, C. Li, M. Jafarzadeh, and T. E. Boulton, "Few-shot class incremental learning leveraging self-supervised features," in *Proceedings of the IEEE Conference on Computer Vision and Pattern Recognition*. IEEE, 2022, pp. 3900–3910.
- [90] A. Gu, K. Goel, and C. Re, "Efficiently modeling long sequences with structured state spaces," in *Proceedings of the International Conference on Learning Representations*, 2021.
- [91] A. Gu, I. Johnson, K. Goel, K. Saab, T. Dao, A. Rudra, and C. Ré, "Combining recurrent, convolutional, and continuous-time models with linear state space layers," in *Proceedings of the Advances in Neural Information Processing Systems*. MIT Press, 2021, pp. 572–585.
- [92] Y. Sun, L. Dong, S. Huang, S. Ma, Y. Xia, J. Xue, J. Wang, and F. Wei, "Retentive network: A successor to transformer for large language models," *arXiv preprint arXiv:2307.08621*, 2023.
- [93] M. Poli, S. Massaroli, E. Nguyen, D. Y. Fu, T. Dao, S. Baccus, Y. Bengio, S. Ermon, and C. Ré, "Hyena hierarchy: Towards larger convolutional language models," in *Proceedings of the International Conference on Machine Learning*. PMLR, 2023, pp. 28 043–28 078.
- [94] J. T. Smith, A. Warrington, and S. Linderman, "Simplified state space layers for sequence modeling," in *Proceedings of the International Conference on Learning Representations*, 2023.
- [95] B. Peng, E. Alcaide, Q. Anthony, A. Albalak, S. Arcadinho, H. Cao, X. Cheng, M. Chung, M. Grella, K. K. GV *et al.*, "Rwkv: Reinventing rns for the transformer era," *arXiv preprint arXiv:2305.13048*, 2023.
- [96] D. Y. Fu, T. Dao, K. K. Saab, A. W. Thomas, A. Rudra, and C. Re, "Hungry hungry hippos: Towards language modeling with state space models," in *Proceedings of the International Conference on Learning Representations*, 2022.
- [97] J. Wang, J. N. Yan, A. Gu, and A. M. Rush, "Pretraining without attention," *arXiv preprint arXiv:2212.10544*, 2022.
- [98] S. Wang and B. Xue, "State-space models with layer-wise non-linearity are universal approximators with exponential decaying memory," *arXiv preprint arXiv:2309.13414*, 2023.
- [99] C. Lu, Y. Schroecker, A. Gu, E. Parisotto, J. Foerster, S. Singh, and F. Behbahani, "Structured state space models for in-context reinforcement learning," *Proceedings of the Advances in Neural Information Processing Systems*, 2024.
- [100] T. Dao and A. Gu, "Transformers are ssms: Generalized models and efficient algorithms through structured state space duality," in *Proceedings of the International Conference on Machine Learning*. PMLR, 2024.
- [101] R. Waleffe, W. Byeon, D. Riach, B. Norick, V. Korthikanti, T. Dao, A. Gu, A. Hatamizadeh, S. Singh, D. Narayanan *et al.*, "An empirical study of mamba-based language models," *arXiv preprint arXiv:2406.07887*, 2024.
- [102] Q. Lv, X. Deng, G. Chen, M. Y. Wang, and L. Nie, "Decision mamba: A multi-grained state space model with self-evolution regularization for offline rl," *arXiv preprint arXiv:2406.05427*, 2024.
- [103] K. Goel, A. Gu, C. Donahue, and C. Ré, "It's raw! audio generation with state-space models," in *Proceedings of the International Conference on Machine Learning*. PMLR, 2022, pp. 7616–7633.
- [104] Y. Zou, S. Zhang, Y. Li, and R. Li, "Margin-based few-shot class-incremental learning with class-level overfitting mitigation," in *Proceedings of the Advances in Neural Information Processing Systems*. MIT Press, 2022, pp. 27 267–27 279.
- [105] Z. Zhong, J. Cui, Y. Yang, X. Wu, X. Qi, X. Zhang, and J. Jia, "Understanding imbalanced semantic segmentation through neural collapse," in *Proceedings of the IEEE Conference on Computer Vision and Pattern Recognition*. IEEE, 2023, pp. 19 550–19 560.
- [106] Z. Li, X. Shang, R. He, T. Lin, and C. Wu, "No fear of classifier biases: Neural collapse inspired federated learning with synthetic and fixed classifier," in *Proceedings of the IEEE International Conference on Computer Vision*. IEEE, 2023, pp. 5319–5329.
- [107] M. Seo, H. Koh, W. Jeung, M. Lee, S. Kim, H. Lee, S. Cho, S. Choi, H. Kim, and J. Choi, "Learning equi-angular representations for online continual learning," in *Proceedings of the IEEE Conference on Computer Vision and Pattern Recognition*. IEEE, 2024, pp. 23 933–23 942.
- [108] R. Xiao, L. Feng, K. Tang, J. Zhao, Y. Li, G. Chen, and H. Wang, "Targeted representation alignment for open-world semi-supervised learning," in *Proceedings of the IEEE Conference on Computer Vision and Pattern Recognition*. IEEE, 2024, pp. 23 072–23 082.
- [109] J. Ma, Y. Niu, J. Xu, S. Huang, G. Han, and S.-F. Chang, "Digeo: Discriminative geometry-aware learning for generalized few-shot object detection," in *Proceedings of the IEEE Conference on Computer Vision and Pattern Recognition*. IEEE, 2023, pp. 3208–3218.
- [110] Y. Yang, S. Chen, X. Li, L. Xie, Z. Lin, and D. Tao, "Inducing neural collapse in imbalanced learning: Do we really need a learnable classifier at the end of deep neural network?" in *Proceedings of the Advances in Neural Information Processing Systems*. MIT Press, 2022, pp. 37 991–38 002.
- [111] V. Pappas, X. Han, and D. L. Donoho, "Prevalence of neural collapse during the terminal phase of deep learning training," *Proceedings of the National Academy of Sciences*, vol. 117, no. 40, pp. 24 652–24 663, 2020.
- [112] O. Russakovsky, J. Deng, H. Su, J. Krause, S. Satheesh, S. Ma, Z. Huang, A. Karpathy, A. Khosla, M. Bernstein *et al.*, "Imagenet large scale visual recognition challenge," *International Journal of Computer Vision*, vol. 115, no. 3, pp. 211–252, 2015.
- [113] A. Krizhevsky, "Learning multiple layers of features from tiny images," 2009.
- [114] C. Wah, S. Branson, P. Welinder, P. Perona, and S. Belongie, "The caltech-ucsd birds-200-2011 dataset," 2011.
- [115] K. He, X. Zhang, S. Ren, and J. Sun, "Deep residual learning for image recognition," in *Proceedings of the IEEE Conference on Computer Vision and Pattern Recognition*. IEEE, 2016, pp. 770–778.
- [116] H. Zhao, Y. Fu, M. Kang, Q. Tian, F. Wu, and X. Li, "Mgsvf: Multi-grained slow versus fast framework for few-shot class-incremental learning," *IEEE Transactions on Pattern Analysis and Machine Intelligence*, vol. 46, no. 3, pp. 1576–1588, 2021.
- [117] J. Deng, W. Dong, R. Socher, L.-J. Li, K. Li, and L. Fei-Fei, "Imagenet: A large-scale hierarchical image database," in *Proceedings of the IEEE Conference on Computer Vision and Pattern Recognition*. IEEE, 2009, pp. 248–255.
- [118] R. R. Selvaraju, M. Cogswell, A. Das, R. Vedantam, D. Parikh, and D. Batra, "Grad-cam: Visual explanations from deep networks via gradient-based localization," in *Proceedings of the IEEE International Conference on Computer Vision*. IEEE, 2017, pp. 618–626.